High-resolution AP-SMALDI mass spectrometry imaging of Drosophila melanogaster

Article *in* International Journal of Mass Spectrometry · April 2017

DOI: 10.1016/j.ijms.2017.04.001

4 authors, including:

Saleh M. Khalil
Justus-Liebig-Universität Gießen
4 PUBLICATIONS **12** CITATIONS

SEE PROFILE

Katja Becker
Justus-Liebig-Universität Gießen
322 PUBLICATIONS **10,499** CITATIONS

SEE PROFILE

International Journal of Mass Spectrometry 416 (2017) 1–19

Contents lists available at ScienceDirect

International Journal of Mass Spectrometry

journal homepage: www.elsevier.com/locate/ijms

High-resolution AP-SMALDI mass spectrometry imaging of *Drosophila melanogaster*

S.M. Khalil[a], J. Pretzel[b], K. Becker[b], B. Spengler[a,*]

[a] Institute of Inorganic and Analytical Chemistry, Justus Liebig University Giessen, Germany
[b] Biochemistry and Molecular Biology, Interdisciplinary Research Center, Justus Liebig University Giessen, Germany

ARTICLE INFO

Keywords:
Drosophila melanogaster
Lipids
Small metabolites
Neuropeptides
High resolution mass spectrometry imaging
AP-SMALDI imaging

ABSTRACT

The pomace fly or fruit fly *Drosophila melanogaster* is known as a cost-effective model organism widely used to study neurological diseases and metabolite-related diseases. Among these metabolites, lipids play important roles in energy homeostasis, metabolism, membrane structure, and signaling. Although the *Drosophila* lipidome has been described in previous studies, there is only a little information on the localization and distribution of the various lipid classes and species in the fly. In this work, high-resolution atmospheric pressure scanning microprobe matrix-assisted laser desorption/ionization (AP-SMALDI) mass spectrometry imaging was performed in order to determine the spatially resolved distribution of metabolites of *D. melanogaster*, with a focus on the tissue-specific characteristic regional distributions of identified compounds from 20 µm thick cryosections of the fly. We identified and characterized the anatomical distribution of a total of 97 lipids, 62 of them identified as glycerophospholipids and sphingolipids and 35 of them as glycerolipids, in three biological replicates of the fly with a consistent anatomical distribution using 2,5-dihydroxybenzoic acid (DHB) as a matrix for soft ionization in positive-ion mode with a pixel size of 5–10 µm. Furthermore, we used *para*-nitroaniline as a matrix for both the positive- and negative-ion mode, enabling the identification of 89 deprotonated lipids in negative-ion mode. Among them, 48 have been identified in both positive- (protonated) and negative-ion (deprotonated) mode within the mass accuracy of ± 3 ppm. All ion images were separated according to their localization principally into head, posterior region and whole body of the fly. The spatial identity especially of *Drosophila* brain metabolites, including lipids, small metabolites and neuropeptides, will provide the possibility of studying neurodegenerative diseases. Therefore, we additionally mapped the distribution of neuropeptides in coronal *Drosophila* brain sections. Furthermore, several lipophilic male- and female-specific sex pheromones were identified, differentiated, and characterized according to their typical distribution pattern in mated and virgin flies. We report on an efficient method for the preparation of improved tissue sections after ethanol dehydration and 5% carboxymethylcellulose and gelatin embedding, capable of maintaining the tissue integrity of the whole fly, which was a challenge due to the hard cuticle and heterogeneous tissue types of this insect. Moreover, our instrumentation with a high spatial resolution, mass resolution and mass accuracy combined with on-tissue MS/MS imaging overcomes common limitations typically observed with low resolution mass spectrometric imaging, such as insufficient spatial resolution which cannot deliver precise and detailed information from the internal organ-specific tissues, and uncertainties of generated signals based on low mass accuracy and resolution. By using DHB, our approach allowed the identification of protonated, sodiated and potassiated lipid species within a mass accuracy of ± 1 ppm and lipophilic pheromones within ± 3 ppm with a spatial resolution set up within 5–15 µm at a high detection sensitivity of the instrumentation.

1. Introduction

The model system fruit fly (*Drosophila melanogaster*), is one of the most popular organisms in biological investigations of numerous developmental and cellular processes. The use of insects as model organisms, due to the reduced complexity of the metabolism of invertebrates compared to vertebrates, simplifies the investigation of biological processes in order to understand fundamental aspects of the cell metabolism. Its characteristic adipose tissues and lipid transport system, makes *D. melanogaster* a close model to humans [1,2] for studying the molecular basis of lipid-related human diseases, such as obesity [3]. Mass spectrometry imaging (MSI) is a novel technique for

* Corresponding author at: Institute of Inorganic and Analytical Chemistry, Heinrich-Buff-Ring 17, Justus Liebig University Giessen, 35392 Giessen, Germany.
E-mail address: Bernhard.Spengler@anorg.Chemie.uni-giessen.de (B. Spengler).

http://dx.doi.org/10.1016/j.ijms.2017.04.001
Received 19 August 2016; Received in revised form 27 December 2016; Accepted 4 April 2017
Available online 08 April 2017
1387-3806/

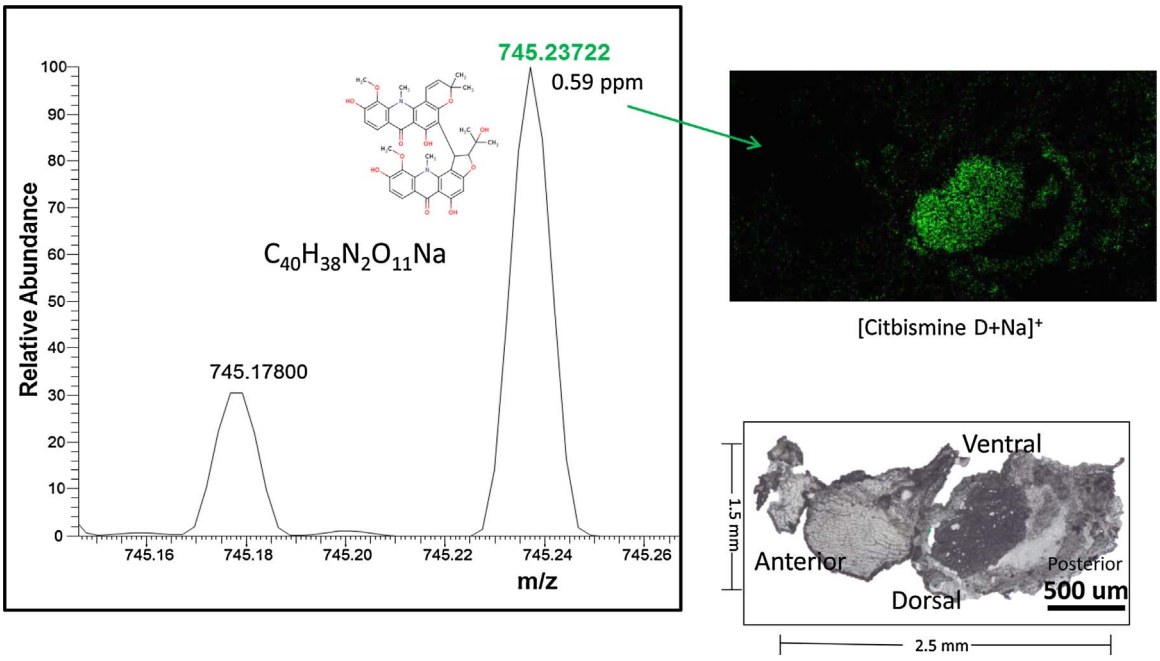

Fig. 1. AP-SMALDI analysis of sodiated 'citbismine D' (*m/z* 745.23722, 0.59 ppm), a yeast-associated compound from rotting citrus fruits. The substance was imaged with 6 μm step size and was found to be localized mostly in the posterior region of a female fly, presumably corresponding to the gut.

the analysis of molecular components directly from tissues. Combined with histological methods, it allows a topographical mapping of molecules identified by mass spectrometry (MS) and provides information about the spatial distribution of these molecules throughout tissues [4]. Moreover, this technique enables a simultaneous analysis of multiple molecules in single cells, tissues, organs, or whole animals [4]. The application ranges from tumor diagnostics, through lipid and protein research, to drug localization studies [5–7].This technique was recently adjusted for the profiling of molecules in insects and mosquitoes [8–12]. The impact and diversity of MS and MSI in lipidomic and metabolomic research is increasing [6,8,12,13]. Lipids have important biological functions in energy homeostasis, membrane structure and fluidity, and signaling processes [14]. Furthermore, lipids play a crucial role as pheromones for the chemical communication of animals. The lipidome of *D. melanogaster*, including pheromones, has been studied well [15,16]. Previous studies of *Drosophila* extracts from different body parts provided important insights about lipids and metabolites, but without any spatial information [17–20]. However, knowledge about the localization of lipids in *D. melanogaster* is still limited. Surface lipids of male and female *D. melanogaster*, i.e. cuticular hydrocarbons, were recently successfully determined by MALDI MSI [21,22]. We provide here a detailed analysis of the spatial distribution of lipids and pheromones in whole body sections of *D. melanogaster*. Moreover, we distinguish between male and female virgin and mated *D. melanogaster* flies and highlight mating-related changes of distribution and intensity of pheromones. A study published recently identified the distribution of six different lipid classes and male-specific pheromones of *D. melanogaster* using elevated-pressure MALDI-MSI, thereby, demonstrating clearly the suitability of this technique for a detailed spatiotemporal mapping of lipids within complex tissue material, such as *D. melanogaster* whole body sections [10]. In extension of that, we could identify lipids and pheromones with higher spatial resolution and with a better mass accuracy, providing a more precise and recurrent localization, by examining the anatomy of different replicates of fruit flies using two different matrix applications. We identified different classes of glycerophospholipids, sphingolipids and glycerolipids. Moreover, we determined the distribution patterns of phospholipids and lipophilic putative pheromones in mated and virgin male and female *D. melanogaster* flies.

Furthermore, *D. melanogaster* is an ideal model organism for studying neurological disorders, e.g. Neumann-Pick disease, epilepsy and Parkinson's disease [23]. Several approaches have been encountered including different MS techniques to analyze *Drosophila* brains or reveal proteomic profiling [24]. Thus, the fruit fly is considered to be one of the major invertebrate model systems in the field of neuroscience. MALDI imaging studies have a great potential to explain the spatial patterns of various biomolecules in diversified research areas of pharmaceuticals, biology and neuroscience [25]. Neuropeptides act in the nervous system as diversified signal molecules that can affect numerous biological processes, including behavior, development, heart rate, metabolism, and reproduction, which were productively studied in *D. melanogaster* [26–28]. MS-based approaches have been previously applied for the detection and identification of neuropeptides from homogenized cells in different developmental lifespans of *D. melanogaster* [27,29–32]. A combination of ToF-SIMS (time-of-flight secondary ion MS) and SEM (scanning electron microscopy) imaging studies on fruit fly brains have recently described the distribution of various intact lipids, including the stimulant drug methylphenidate [33,34]. Using SIMS it was possible to image with a pixel size of 3 μm, but the mass resolution was not sufficient to identify compounds. Here, we performed high-resolution AP-SMALDI MSI in order to study the brain of *D. melanogaster*, which enabled the specific localization and accurate identification of various biomolecules, including neuropeptides. Moreover, we present an MSI-friendly method for gelatin embedding and preparation of 20 μm sections from the brain of *D. melanogaster*, being smaller than 1 mm in diameter. Fruit fly brains of biological replicates were analyzed to obtain their structural identity reproducibly.

2. Experimental

2.1. Materials and methods

2.1.1. Chemicals

DHB (98% purity) was purchased from Sigma-Aldrich (Taufkirchen, Germany). Paranitroaniline (pNA) was purchased from Sigma-Aldrich

Table 1
Phospholipids and glycerolipids detected in AP-SMALDI MSI analyses of male and female *Drosophila melanogaster* in positive ion mode using DHB as a matrix. Structures were assigned based on accurate mass and database information from METLIN and LIPID MAPS.

Formula	$[M+H]^+_{calc}$	$[M+Na]^+_{calc}$	$[M+K]^+_{calc}$	RMSE (root mean square error)of $[M+K]^+$obs./ppm	Assignment
Head region					
$C_{40}H_{80}NO_8P$	734.56943	756.55137	772.52531	−0.26	PC(32:0)
$C_{44}H_{86}NO_7P$	772.62147	794.60341	810.57735	0.80	PC(O-36:2)/PC(P-36:1)
$C_{41}H_{82}NO_8P$	748.58508	770.56703	786.54097	−0.35	PE(36:0)
$C_{41}H_{80}NO_7P$	730.57452	752.55646	768.53040	−0.49	PE(O-36:2)/PE(P-36:1)
$C_{41}H_{78}NO_7P$	728.55887	750.54081	766.51475	0.82	PE(O-36:3)/PE(P-36:2)
$C_{44}H_{80}NO_7P$	766.57452	788.55646	804.53040	0.76	PC(O-36:4)/PC(P-36:3)
$C_{36}H_{71}N_2O7P$	675.50717	697.48911	713.46305	−0.77	PE-Cer(34:2)
$C_{38}H_{77}N_2O_6P$	689.55920	711.54115	727.51508	−0.90	PE-Cer(36:1)
Gut region					
$C_{27}H_{53}NO_4$	456.40474	478.38668	494.36062	0.55	Arachidyl Carnitine
$C_{36}H_{69}NO_3$	564.53502	586.51696	602.49090	−0.85	Cer(36:2)
$C_{36}H_{70}NO_8P$	676.49118	698.47313	714.44707	−0.19	PC(28:1)
$C_{38}H_{74}NO_8P$	704.52248	726.50443	742.47837	−0.09	PC(30:1)
$C_{38}H_{72}NO_8P$	702.50683	724.48878	740.46272	−0.37	PC(30:2)
$C_{40}H_{75}O_{10}P$	747.51706	769.49901	785.47295	0.51	PG(34:2)
$C_{38}H_{66}NO_{10}P$	728.44971	750.43166	766.40559	−0.52	PS(32:4)
$C_{40}H_{72}NO_{10}P$	758.49666	780.47861	796.45255	−0.46	PS(34:3)
$C_{42}H_{78}NO_{10}P$	788.54361	810.52556	826.49950	−0.04	PS(36:2)
$C_{42}H_{74}NO_{10}P$	784.51231	806.49426	822.46820	−0.63	PS(36:4)
$C_{25}H_{50}NO_7P$	508.33977	530.32171	546.29565	1.10	LysoPE(20:1)
$C_{43}H_{79}O_{12}P$	819.53819	841.52014	857.49408	−0.76	PI(P-34:2)
whole body					
$C_{21}H_{42}NO_7P$	452.27717	474.25911	490.23305	0.67	LPE(16:1)
$C_{21}H_{44}NO_7P$	454.29282	476.27476	492.24870	0.71	LPE(16:0)
$C_{26}H_{48}NO_7P$	518.32412	540.30606	556.28000	0.03	LPC(18:3)
$C_{26}H_{50}NO_7P$	520.33977	542.32171	558.29565	−0.20	LPC(18:2)
$C_{26}H_{52}NO_7P$	522.35542	544.33736	560.31130	−0.22	LPC(18:1)
$C_{26}H_{54}NO_7P$	524.37107	546.35301	562.32695	0.03	LPC(18:0)
$C_{28}H_{52}NO8P$	562.35033	584.33228	600.30622	0.22	LPC(20:2)
$C_{28}H_{54}NO_8P$	564.36598	586.34793	602.32187	0.25	LPC(20:1)
$C_{36}H_{72}NO_8P$	678.50683	700.48878	716.46272	0.13	PC(28:0)
$C_{34}H_{66}NO_{10}P$	680.44971	702.43166	718.40559	−0.54	PS(28:0)
$C_{42}H_{79}O_{10}P$	688.49118	710.47313	726.44707	0.09	PE(32:2)
$C_{42}H_{79}O_{10}P$	690.50683	712.48878	728.46272	0.13	PE(32:1)
$C_{36}H_{71}O_{10}P$	695.48576	717.46770	733.44164	−0.75	PG(30:0)
$C_{36}H_{66}NO_{10}P$	704.44971	726.43166	742.40559	0.18	PS(30:2)
$C_{36}H_{68}NO_{10}P$	706.46536	728.44731	744.42125	−0.15	PS(30:1)
$C_{39}H_{72}NO_8P$	714.50683	736.48878	752.46272	0.46	PE(34:3)
$C_{39}H_{74}NO_8P$	716.52248	738.50443	754.47837	0.25	PE(34:2)
$C_{42}H_{79}O_{10}P$	718.53813	740.52008	756.49402	0.32	PE(34:3)
$C_{38}H_{68}NO_{10}P$	730.46536	752.44731	768.42125	−0.29	PS(32:3)
$C_{40}H_{76}NO_8P$	730.53813	752.52008	768.49402	−0.27	PC(32:2)
$C_{38}H_{70}NO_{10}P$	732.48101	754.46296	770.43690	−1.17	PS(32:2)
$C_{40}H_{78}NO_8P$	732.55378	754.53573	770.50967	0.39	PC(32:1)
$C_{41}H_{72}NO_8P$	738.50683	760.48878	776.46272	−0.74	PE(36:5)
$C_{42}H_{79}O_{10}P$	742.53813	764.52008	780.49402	0.38	PE(36:3)
$C_{41}H_{78}NO_8P$	744.55378	766.53573	782.50967	0.10	PE(36:2)
$C_{42}H_{79}O_{10}P$	744.55378	766.53573	782.50967	0.10	PE(36:2)
$C_{42}H_{79}O_{10}P$	746.56943	768.55138	784.52532	0.22	PE(36:1)
$C_{42}H_{76}NO_8P$	754.53813	776.52008	792.49402	−0.04	PC(34:4)
$C_{40}H_{70}NO_{10}P$	756.48101	778.46296	794.43690	−0.81	PS(34:4)
$C_{42}H_{78}NO_8P$	756.55378	778.53573	794.50967	−0.18	PC(34:3)
$C_{42}H_{80}NO_8P$	758.56943	780.55137	796.52531	0.01	PC(34:2)
$C_{42}H_{82}NO_8P$	760.58508	782.56703	798.54097	−0.21	PC(34:1)
$C_{42}H_{79}O_{10}P$	770.56943	792.55138	808.52532	0.09	PE(38:3)
$C_{42}H_{79}O_{10}P$	771.51706	793.49901	809.47295	−0.95	PG(36:4)
$C_{42}H_{79}O_{10}P$	772.58508	794.56703	810.54097	0.28	PE(38:2)
$C_{42}H_{79}O_{10}P$	774.60073	796.58268	812.55662	0.41	PE(38:1)
$C_{44}H_{80}NO_8P$	782.56943	804.55138	820.52532	0.08	PC(36:4)
$C_{44}H_{82}NO_8P$	784.58508	806.56703	822.54097	0.10	PC(36:3)
$C_{44}H_{84}NO_8P$	786.60073	808.58268	824.55662	0.55	PC(36:2)
$C_{44}H_{86}NO_8P$	788.61638	810.59833	826.57227	0.32	PC(36:1)
$C_{46}H_{88}NO_8P$	814.63203	836.61398	852.58792	0.02	PC(38:2)
$C_{46}H_{90}NO_8P$	816.64768	838.62963	854.60357	−0.03	PC(38:1)
Glycerolipids (present in whole body)					
$C_{23}H_{38}O_4$	379.28429	401.26623	417.24017	−0.77	MG(20:4)
$C_{23}H_{40}O_4$	381.29994	403.28188	419.25582	−0.58	MG(20:3)
$C_{33}H_{60}O_5$	537.45135	559.43330	575.40723	−0.05	DG(30:2)
$C_{35}H_{62}O_5$	563.46700	585.44894	601.42288	−0.88	DG(32:3)

(continued on next page)

Table 1 *(continued)*

Formula	$[M+H]^+_{calc}$	$[M+Na]^+_{calc}$	$[M+K]^+_{calc}$	RMSE (root mean square error)of $[M+K]^+$obs./ppm	Assignment
$C_{35}H_{64}O_5$	565.48265	587.46460	603.43853	−0.06	DG(32:2)
$C_{35}H_{66}O_5$	567.49830	589.48025	605.45418	−0.11	DG(32:1)
$C_{35}H_{68}O_5$	569.51395	591.49590	607.46983	−0.06	DG(32:0)
$C_{37}H_{64}O_5$	589.48265	611.46460	627.43853	−0.28	DG(34:4)
$C_{37}H_{66}O_5$	591.49830	613.48025	629.45418	−0.10	DG(34:3)
$C_{37}H_{68}O_5$	593.51395	615.49590	631.46983	−0.35	DG(34:2)
$C_{37}H_{70}O_5$	595.52960	617.51155	633.48548	−0.46	DG(34:1)
$C_{39}H_{68}O_5$	617.51395	639.49590	655.46983	−0.55	DG(36:4)
$C_{39}H_{70}O_5$	619.52960	641.51155	657.48548	0.44	DG(36:3)
$C_{39}H_{72}O_5$	621.54525	643.52720	659.50113	−0.44	DG(36:2)
$C_{39}H_{70}O_6$	635.52452	657.50646	673.48040	−0.01	TG(36:2)
$C_{39}H_{72}O_6$	637.54017	659.52211	675.49605	0.02	TG(36:1)
$C_{41}H_{76}O_5$	649.57655	671.55850	687.53243	−0.56	DG(38:2)
$C_{49}H_{92}O_6$	777.69667	799.67861	815.65255	0.21	TG(46:1)
$C_{51}H_{92}O_6$	801.69667	823.67861	839.65255	−0.05	TG(48:3)
$C_{51}H_{94}O_6$	803.71232	825.69426	841.66820	−0.02	TG(48:2)
$C_{53}H_{96}O_6$	829.72797	851.70991	867.68385	−0.01	TG(50:3)
$C_{53}H_{98}O_6$	831.74362	853.72556	869.69950	0.00	TG(50:2)
$C_{55}H_{102}O_6$	859.77492	881.75686	897.73080	−0.15	TG(52:2)
$C_{57}H_{96}O_6$	877.72797	899.70991	915.68385	0.00	TG(52:4)
$C_{51}H_{96}O_6$	805.72797	827.70991	843.68385	0.42	TG(48:1)
$C_{43}H_{80}O_6$	693.60277	715.58471	731.55865	−0.20	TG(40:0)
$C_{43}H_{82}O_6$	695.61842	717.60036	733.57430	−0.27	TG(40:1)
$C_{45}H_{84}O_6$	721.63407	743.61601	759.58995	−0.23	TG(42:1)
$C_{45}H_{86}O_6$	723.64972	745.63166	761.60560	0.13	TG(42:0)
$C_{47}H_{86}O_6$	747.64972	769.63166	785.60560	0.05	TG(44:2)
$C_{47}H_{88}O_6$	749.66537	771.64731	787.62125	0.18	TG(44:1)
$C_{49}H_{88}O_6$	773.66537	795.64731	811.62125	0.17	TG(46:3)
$C_{49}H_{90}O_6$	775.68102	797.66296	813.63690	0.40	TG(46:2)
$C_{55}H_{100}O_6$	857.75927	879.74121	895.71515	−0.08	TG(52:3)
$C_{39}H_{68}O_6$	633.50887	655.49081	671.46475	−0.09	TG(36:3)

(Taufkirchen, Germany). Glass microscope slides (ground edged, frosted, 75 × 25 × 1 mm) were obtained from VWR International (Darmstadt, Germany), and carboxymethylcellulose (CMC) sodium salt from Sigma Aldrich (Taufkirchen, Germany). Trifluoroacetic acid (TFA) and water (HPLC grade) were purchased from Fluka (Neu Ulm, Germany). All chemicals used in this study were of the highest purity available.

2.1.2. Drosophila husbandry

D. melanogaster w118 lacking the eye pigments were maintained at 25 °C on a standard diet containing cornmeal, sugar, yeast, destilled water, propionic acid, nipagin, and beet syrup. Virgin male and female flies were collected and separated by sex within six hours after hatching, immediately frozen in liquid nitrogen and stored at −80 °C until cryosectioning. Mated male and female flies were collected and separated by sex six days after hatching, frozen in liquid nitrogen and stored at −80 °C until cryosectioning.

2.1.3. Cryosectioning of Drosophila melanogaster

D. melanogaster w118, of approximately 2–2.5 (h) × 1–1.5 mm (w) size, were systematically and consistently prepared for this MSI study. To the best of our knowledge, there is no recommended protocol for the preparation of *D. melanogaster* whole body sections for MSI studies. Reproducible sample preparation of this tiny fly is especially complicated due to its external and internal anatomy and the hydrophobic external cuticle [10].

As a first step, we removed the wings and legs using forceps and knives and then soaked the flies in Petri dishes filled with 40, 70 and 100% of ethanol, respectively, for 10 min each and let them dry. Ethanol facilitates dehydration of the insects, hardens their internal tissue and helps to keep the integrity of the whole insect morphology after sectioning. Tissue sections were not again soaked in ethanol, as ethanol penetrates the cuticle of the fly. Ethanol treatment might have some effects on cuticular lipids, which are more polar and easily soluble in polar solvents such as ethanol. The insect body is fragile and it is impossible to make slices without the support of embedding media [35]. Therefore, a recommended embedding material, such as CMC was used, which does not interfere with the detection sensitivity of molecular compounds in MALDI-MSI, as other supporting material like Optimal Cutting Temperature (OCT) compound do [36–38]. We tested CMC in trial sectioning of insects and it was found that 5% of CMC works best in order to obtain suitable sections for MSI studies. It reduces movement after pouring the flies on to it and helps to maintain the coverage and integrity of the whole body of the fly. Ionization efficiency depends partially on the thickness of the tissue slices and 5–20 μm of tissue sections are generally chosen to study low molecular weight compounds [39]. We prepared 20 μm sections from both male and female flies for high-resolution MSI of wild type *D. melanogaster* in the mass range of m/z = 200–1000.

In the second step of our preparation protocol, flies soaked with ethanol were fixed in Cryomolds® cast blocks (15 × 15 × 5 mm) with 5% CMC embedding solution. Half of the plastic block was firstly filled with 5% CMC. The flies were then placed firmly in the middle of the block. Care was taken to reduce the movement of the flies during the placement. The block with flies was left for about 30 min at −80 °C to fix them in place. Additional CMC was poured on top to cover the fixed flies and the samples were again left at −80 °C for at least 24 h. During this time, CMC with fixed flies adapts a waxy texture, which is suitable for sectioning. The plastic blocks containing *D. melanogaster* were then put into the cryochamber at −23 to −25 °C for about 10–15 min to equilibrate with the chamber temperature. The *D. melanogaster* samples were then sliced into sections of 20 μm thickness with a cryotome (HM 525 Cryostat, Thermo Scientific, Dreieich, Germany). Longitudinal sections were made from whole body *D. melanogaster* on a cryotome holder. Sections were thaw-mounted on frosted glass slides with ground edges (75 × 25 × 1 mm) and immediately measured after matrix application or stored at −80 °C for later imaging studies. In each case, the sections were put into a desiccator for at least 20 min prior to

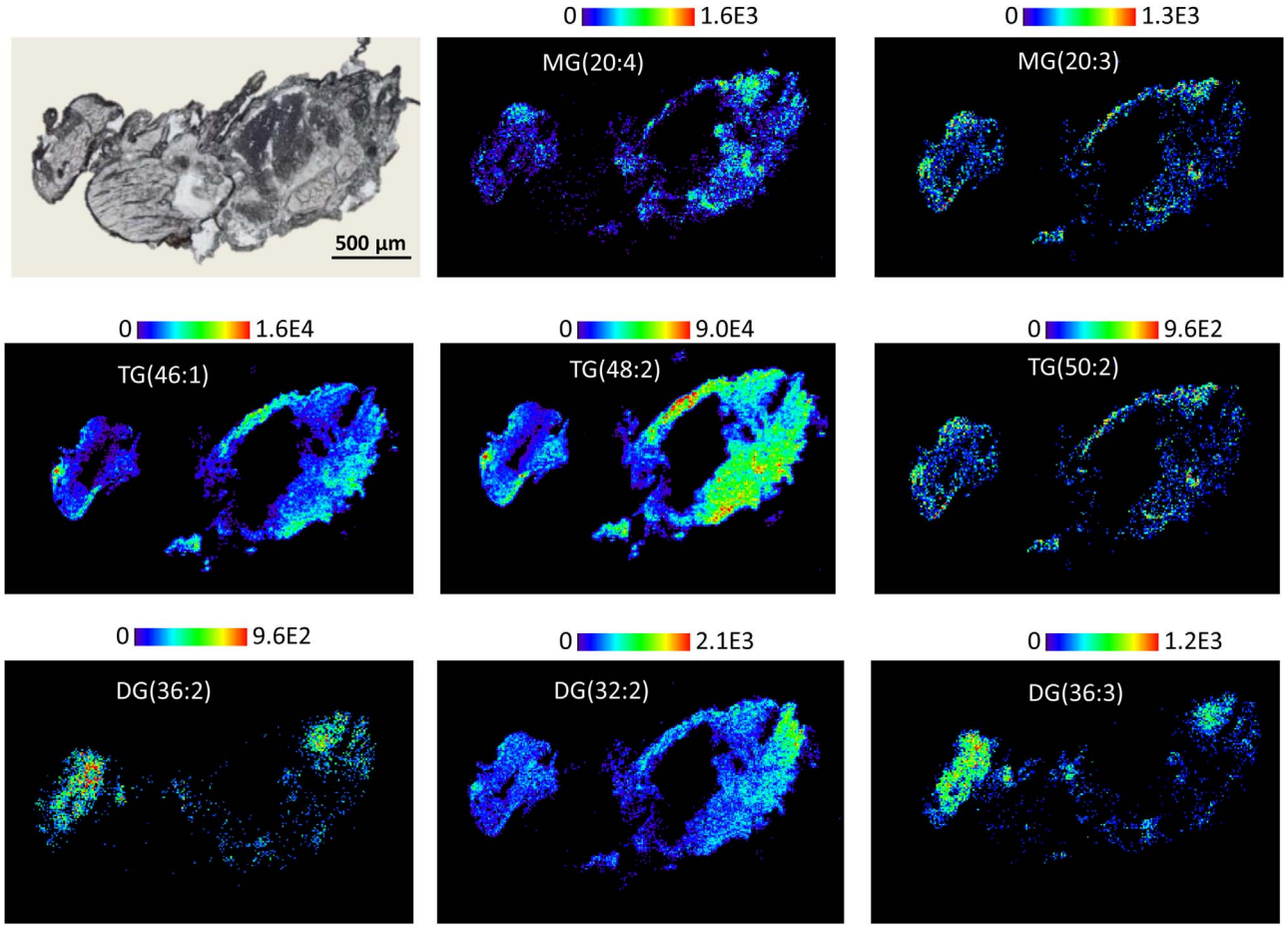

Fig. 2. AP-SMALDI positive-ion pseudocolor images of three classes of glycerolipids, triglycerides (TG), diglycerides (DG), and monoglycerides (MG). Distributions of these lipids were found to be prominent in head and abdomen of *D. melanogaster*. Glycerolipids were detected as sodiated and potassiated species in all cases. All images were created by adding signal intensities of the two ion species $[M+Na]^+$, and $[M+K]^+$ in one image. The resolution was set to 10 µm per pixel (10 µm step size) and the size of the measurement was 312 × 150 pixels.

measurement, to avoid the process of condensation and humidity on the surface of the samples. The overall sample preparation method is summarized in Supplementary Fig. S1.

2.1.4. Optical microscopy

Optical images of 20 µm *D. melanogaster* tissue sections were taken before matrix application with an Olympus BX-41 microscope (Olympus Europa GmbH, Hamburg, Germany) at a microscopic magnification of 5x. Optical images of the laser burn patterns were taken after each measurement to determine the precise laser ablation spot size for defined lateral resolution.

2.1.5. Matrix application

The coating of samples with an appropriate matrix plays a crucial role in MALDI-MSI soft ionization [40,41]. The imaging of lipids and metabolites was performed in both positive and negative ion mode. For that purpose, 150 µl of DHB and pNA solutions were homogeneously deposited by a "SMALDI Prep" matrix preparation system (TransMIT GmbH, Giessen, Germany). DHB solution consisted of 30 mg/ml of DHB in 50:50 (v/v) Aceton:H_2O (0.1% TFA). pNA solution consisted of 10 mg/ml of pNA in 50:50 (v/v) Aceton:H_2O. The crystal size of the matrix on the tissue sections was microscopically controlled to be homogeneous and not larger than 5 µm. No washing steps were applied prior to matrix application.

DHB is widely used as a suitable matrix for the analysis of small molecular-weight compounds, such as lipids and metabolites, in the positive ion mode. Protonated ions, sodium adduct ions and potassium adduct ions are mostly observed from biological samples after applying DHB with meaningful biological images [42,43]. On the other hand, pNA was first introduced for lipids in 1995 [44] and is supposed to produce higher signal-to-noise ratios than DHB in both positive- and negative-ion mode under atmospheric pressure for protonated and deprotonated lipid species [45].

2.2. Instrumentation

All imaging experiments were accomplished by using an AP-SMALDI MSI system (AP-SMALDI10®, TransMIT GmbH, Giessen, Germany) coupled to a Fourier transform orbital trapping mass spectrometer (Q Exactive™, Thermo Fisher Scientific GmbH, Bremen, Germany), providing high resolution in mass and space [46]. The laser beam was focused by a centrally bored objective lens to an ablation diameter of 5 µm [47]. Samples were scanned with step sizes (pixel sizes) between 6 and 15 µm for *D. melanogaster* sections of 2–2.5 (h) × 1–1.5 mm (w) size. The Q Exactive instrument was operated in positive-ion mode and in the mass range of m/z = 300-1000. Matrix peaks were used for internal calibration resulting in a mass accuracy of better than ± 1 ppm. The laser beam was focused carefully to avoid oversampling. Automatic gain control was turned off and C-trap injection time was fixed to 500 ms. Ions formed by 30 laser pulses per spot were accumulated in the C-trap prior to detection. The mass resolving power was set to 140,000 at m/z = 200 providing accurate

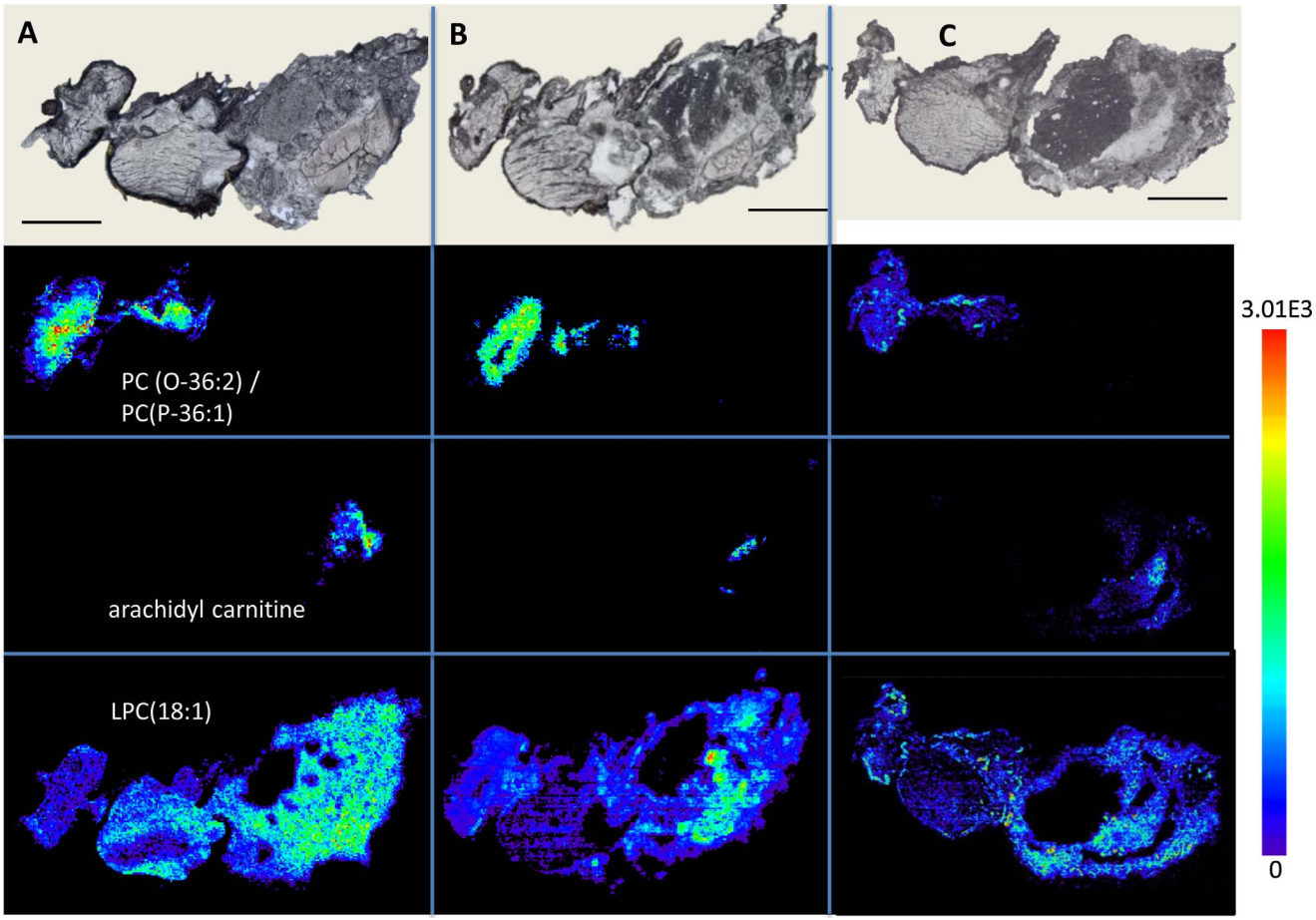

Fig. 3. AP-SMALDI positive-ion pseudocolor images obtained from sections of three female adult *D. melanogaster* A) (272 × 172 pixels, 10 µm per pixel B) 312 × 212 pixels, 10 µm per pixel and C) 494 × 254 pixels, 6 µm per pixel resp.) using DHB as a matrix. Spatial distributions were found to be similar for the three biological replicates for ether phosphatidylcholines PC(O-36:2)/PC(P-36:1) (potassium attached *m/z* 810.57799, 0.79 ppm) in the head, for arachidyl carnitine (potassium attached *m/z* 494.36062, 0.54 ppm) and for LPC(18:1) (potassium attached *m/z* 560.31130, −0.22 ppm). All images were created by adding signal intensities of the three ion species $[M+H]^+$, $[M+Na]^+$, and $[M+K]^+$ in one image. The scale bar for each image represents 500 µm.

mass for determination of elemental compositions.

2.2.1. Image processing

The software package 'MIRION' [48] was used to generate mass images from Q Exactive raw files with a bin width of $\Delta m/z$ = 0.01 or ± 5 ppm. It can discriminate *m/z* images based on mass defect and pixel coverage. Mass spectra from 6 to 15 µm/pixel were obtained in our experiments and all lipid ions were assigned within a mass accuracy of ± 1 ppm. By using the 'MIRION' software package, gray scale images, false color images or RGB (red-green-blue) images are generated from individual lipid ion species (Supplementary Fig. S2).

The 'rainbow pseudocolor' *m/z* images were normalized to the highest intensity for each individual lipid ion species per image. In order to compare the abundances of lipids, the signals of protonated, sodiated and potassiated species of each lipid were summed and presented as one image. No further data processing steps were applied during image generation. Theoretical *m/z* values of each lipid species assigned from the database (www.lipidmaps.org) were used for image generation with a bin width of ± 5 ppm relative to the theoretical value. Each proton-, sodium- or potassium-attached lipid species with less than ± 1 ppm mass error versus the database entry was selected.

2.2.2. Molecular identification directly from tissue

On-tissue AP-SMALDI MS/MS studies were performed directly from fruit fly tissue sections in order to identify the lipids and metabolites after isolation of precursor ions with an isolation width of ± 0.50 u. The laser was scanned with 10–20 µm step size on the tissue for desorption/ionization of precursors. The precursor ions selected and the product ions obtained by high energy collision-induced dissociation (HCD) were ejected from the C-trap and analyzed in the orbitrap. The normalized collision energy for inducing fragmentation in the orbitrap was set to an instrument-specific value of 20–30% in both positive- and negative-ion mode. The HCD fragment ions were detected in the orbitrap at a mass resolution of 35,000–70,000 at *m/z* 200. Fragmentation based on neutral loss from the head group of the phospholipid structure was commonly observed in positive-ion mode HCD experiments (Supplementary Figs. S3 and S4). By performing MS/MS in a negative-ion mode, it was possible to fragment lipids in terms of negative ion loss from the precursor (Supplementary Figs. S5–S7).

3. Results and discussion

3.1. High-resolution AP-SMALDI imaging in positive-ion mode

Our instrumentation enables the combination of high mass and lateral resolution in MSI allowing the delineation of distinct species of phospholipids, neuropeptides and drug compounds from diversified tissue sections with high spatial resolution [49]. Here, we investigated whole body sections of *D. melanogaster* and obtained mass spectrometric images using this approach. A total of 97 phospholipids were identified

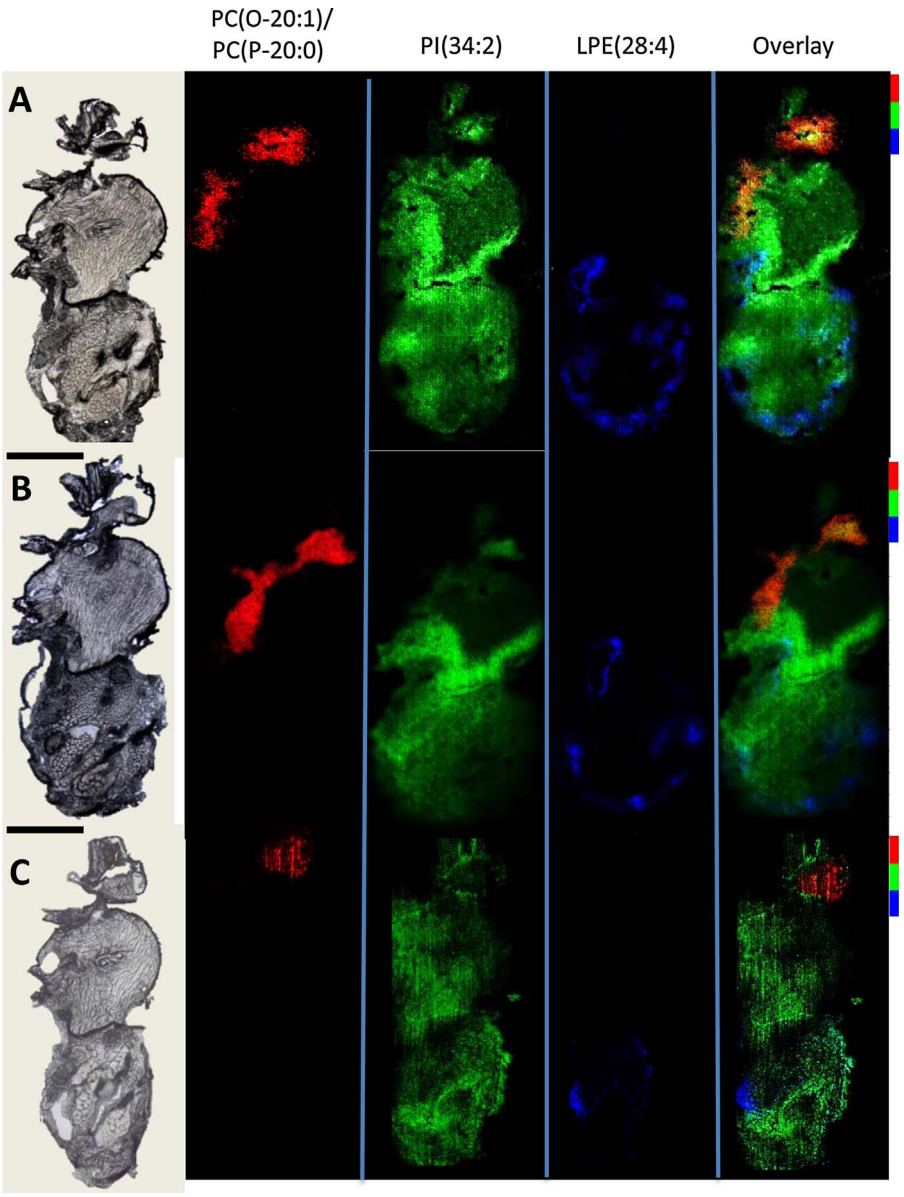

Fig. 4. Negative-ion mode AP-SMALDI images of deprotonated phospholipids ($[M-H]^-$) from three adjacent whole body sections A), B), and C) showing the specific distributions within head, whole body and cuticle of a female fly, acquired using pNA as a matrix. Red: ether lipid phosphatidylcholine PC(O-20:1)/PC(P-20:0) (deprotonated m/z 548.37163, 1.01 ppm), green: phosphatidylinositol PI(34:2) (deprotonated m/z 833.51804, 0.69 ppm), blue: lysophosphatidylinositol LPE(28:4) (deprotonated m/z 619.28817, 0.35 ppm). Images were generated with a bin width of $\Delta m/z = 0.01$ at a mass resolving power of 140,000 at $m/z = 200$ and a mass accuracy of better than 3 ppm. The resolution was set to 8 μm per pixel (8 μm step size) and the size of the three measurements was 416 × 150 pixels, 375 × 148 pixels and 398 × 152 pixels, respectively. The red, green and blue images were overlaid to one RGB image on the right. The scale bar represents 500 μm. (For interpretation of the references to colour in this figure legend, the reader is referred to the web version of this article.)

after DHB application, including glycerophospholipids, sphingolipids and glycerolipids, based on the three major ion species of singly charged protonated, sodiated and potassiated lipids. Glycerophospholipids are the major structural lipids of cells, essential constituents of cell membranes in eukaryotes and play an important role in many membrane activities, such as transport, energy exchange, signal transduction, fluidity, and permeability [17,50,51]. The focus of this study was to identify the diversified lipid, metabolite and neuropeptide classes by higher spatial and mass resolution MSI in the different anatomical structures of the fly. An average mass spectrum acquired in an imaging experiment of a whole female fly is shown in Supplementary Fig. S8. Lipid peak signals are assigned based on accurate mass measurements within the mass accuracy of better than 1 ppm.

We performed MSI of a female adult *D. melanogaster* fly at al resolution of 6 μm pixel size. The precise distribution of metabolites in various tissue regions of the fly are shown in Supplementary Fig. S2 for the case of three selected phospholipid signals. The most intense signal within the whole body of the fly was observed for sodiated PC(34:2) (m/z 780.55138, green, 0.013 ppm). The head of the fly is characterized by the sodiated ether lipid compound PC(O-36:2)/PC(P-36:1) (m/z 794.60338, red, 0.79 ppm) and the posterior region is characterized by one of the monounsaturated protonated phosphatidylcholines, PC(30:1) (m/z 704.52210, blue, 0.08 ppm). The microscopic image of a burn pattern in Supplementary Fig. S9 clearly demonstrates the 6 μm lateral resolution. A 6 μm single pixel mass spectrum from the same fly in a narrow mass window of 752.50-752.60 is shown in Supplementary Fig. S10. Two molecular species of lipids with specific topographical distributions and a mass difference of 35 mDa were clearly separated.

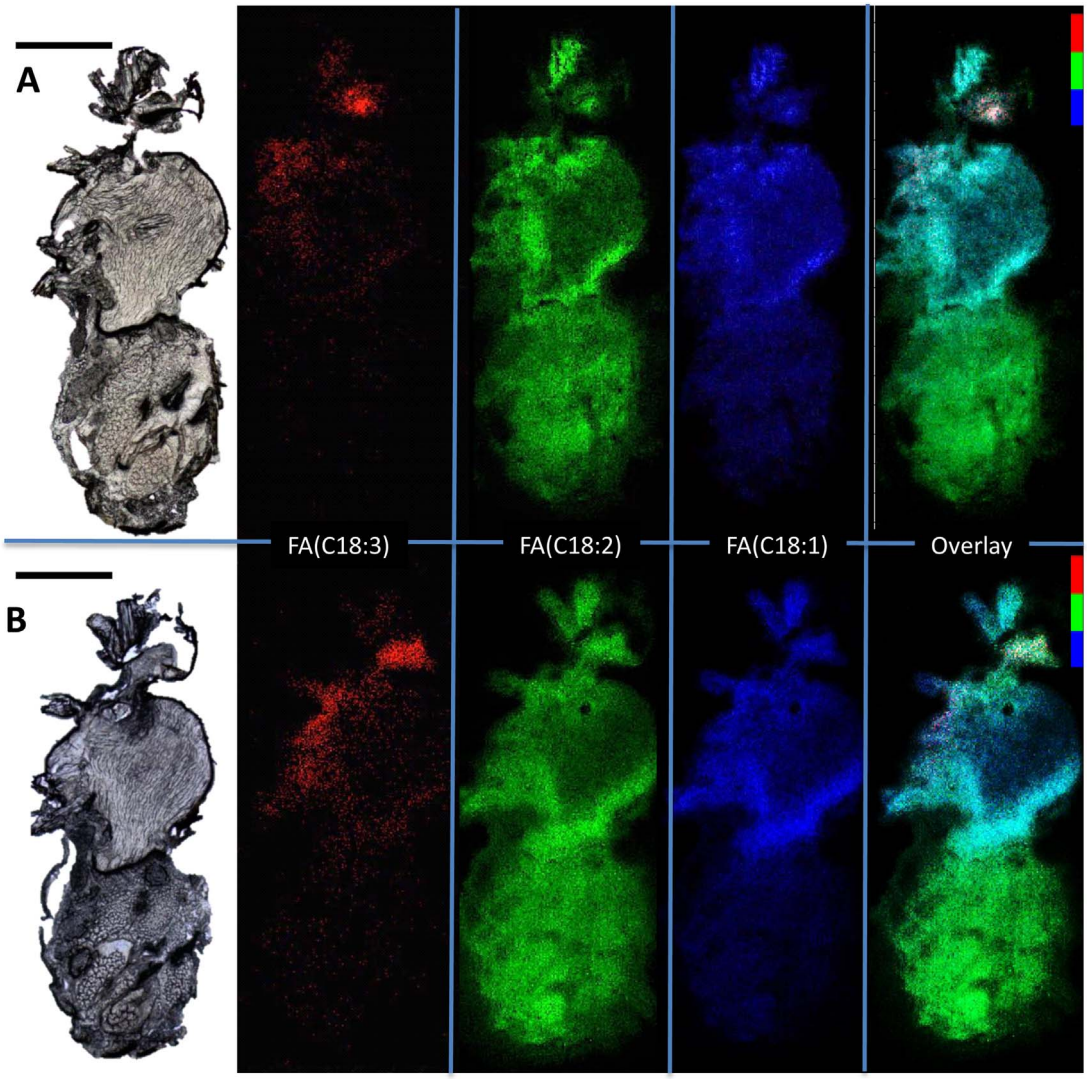

Fig. 5. Negative-ion mode AP-SMALDI images of deprotonated fatty acids ($[M-H]^-$) from two adjacent sections A) and B) of a female fly, acquired using pNA as a matrix. Red: FA(C18:3) (deprotonated m/z 277.21697, 2.75 ppm), green: FA(C18:2) (deprotonated m/z 279.23170, 2.75 ppm), blue: FA(C18:1) (deprotonated m/z 281.24711, −1.39 ppm). The size of the two measurements was 416 × 150 pixels and 375 × 148 pixels, respectively. The red, green and blue images were overlaid to one RGB image on the right. The scale bar represents 500 μm. (For interpretation of the references to colour in this figure legend, the reader is referred to the web version of this article.)

Sodium-attached PC(32:2) and plasmalogen PE(O-36:2)/PE(P-36:1) were imaged using a narrow mass bin width of $\Delta m/z = 0.01$, showing specific distributions in the whole body and especially in the head and extending neuronal tissue of *D. melanogaster*. Ion images generated with such a small bin width of $\Delta m/z = 0.01$ enable to resolve the two distributions of the compounds neighboring in mass by 35 mDa. Such separation is not possible with larger bin widths as typically used by lower-mass-resolution instruments. The effect of using different bin widths for the generation of ion images has been discussed earlier in detail [46,49,52].

A citrus fruit derivative 'citbismine D' was identified and imaged with a lateral resolution of 6 μm per pixel as a sodium-attached ion (Fig. 1). This probably nutrition-derived metabolite was found prominently within the posterior region of the fly, most likely corresponding to the gut region of the female adult fly. High-resolution AP-SMALDI MSI will be applied in the future to study the mechanism of action and effects of e.g. orally administered drugs, metabolites and pesticides.

Glycerolipids, i.e. triglycerides (TGs), diglycerides (DGs) and monoglycerides (MGs), are stored as lipid droplets in the fat body of the fly. Fat bodies enriched mostly with TGs have a major role in the central storage of nutrients and energy fuel surrounded by phospholipids. Energy metabolism in insects is maintained by lipolytic enzymes, i.e. TG lipase, and the hydrolytic activity and conversion of TGs into DGs and MGs occur after the loss of fatty acids (FAs) from the structure. Metabolic activity by MG lipase promotes the loss of glycerol from MGs into FAs [53]. By using our AP-SMALDI approach at a spatial resolution of 10 μm, three glycerolipid classes could be demonstrated within the very high mass accuracy of ± 1 ppm. A total of 35 glycerolipids were identified based on a similar distribution of sodiated and potassiated species with summed FA chain lengths of C20 to C52 (Table 1). Triglycerides were profoundly present, besides di- and monoglycerides in all replicates of female flies examined. TGs were sensitively detected in the present MSI approach, suggesting the possibility to detect sex specific TGs, widely conserved in *D. melanogaster* and mediating mating behavior [54]

Fig. 2 depicts selected pseudocolor images of the three classes of glycerolipids, obtained with 10 μm step size of a female *Drosophila* fly. MS/MS experiments were performed directly on a female fly section for

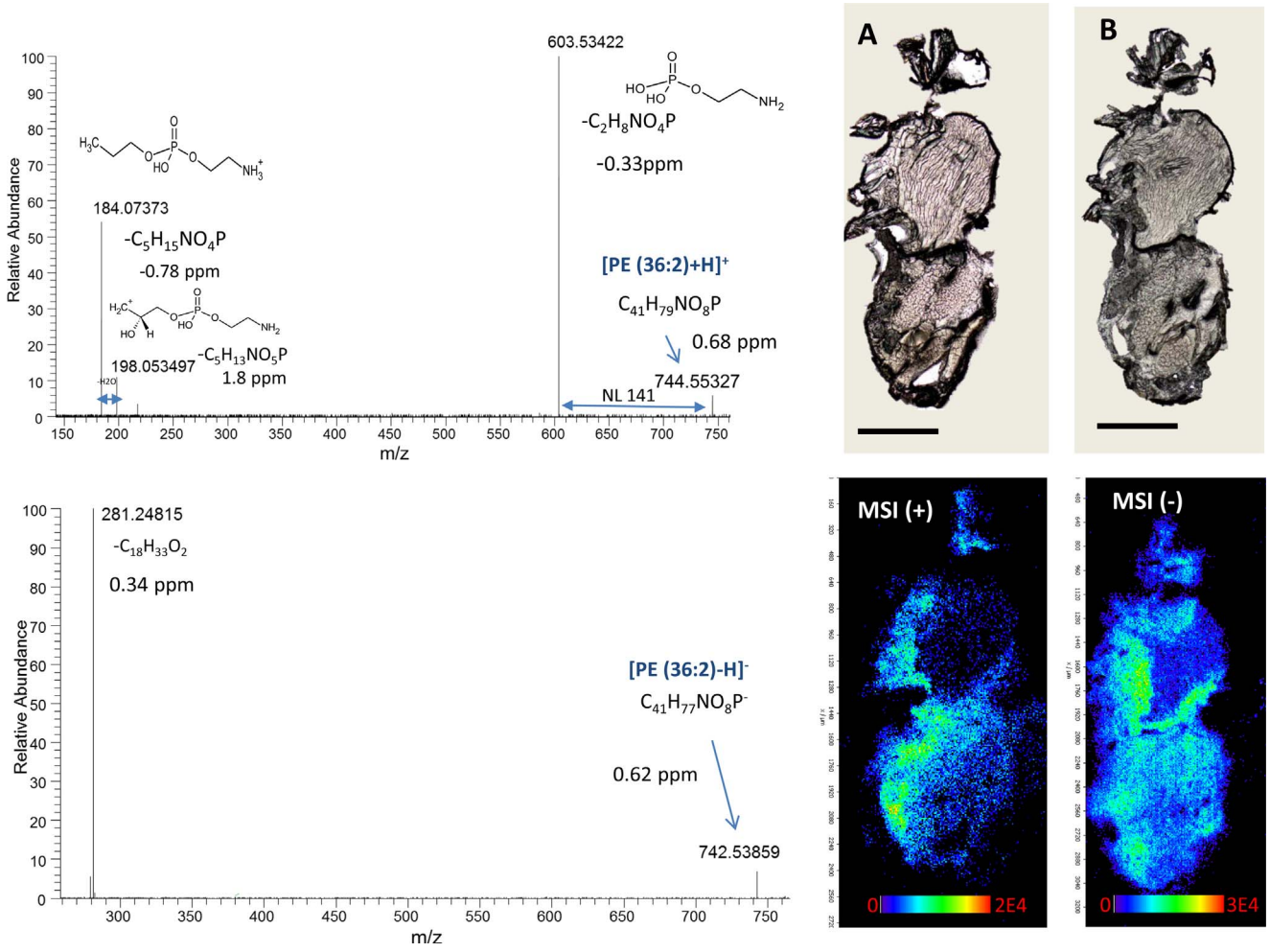

Fig. 6. AP-SMALDI images and on-tissue MS/MS of protonated (positive-ion mode) A) and deprotonated (negative-ion mode) B) phosphotidylethanolamine, PE(36:2) (protonated *m/z* 744.55327, −0.33 ppm and deprotonated *m/z* 742.53859, 0.62 ppm) using pNA as a matrix. Characteristic fragment ions were observed after high-energy collision-induced dissociation (HCD). Similar spatial distributions were observed for the two adjacent sections. The scale bar represents 500 µm.

selected lipid species at a high collision dissociation of 20–30 eV and a mass window of ± 0.5 u using the Q Exactive mass spectrometer in positive-ion mode. The MS/MS of precursor ion *m/z* = 824.55637 resulted in characteristic product ions at *m/z* = 162.95550, *m/z* = 641.49023 $[M–183 + K]^+$ and *m/z* = 765.48199 (neutral loss of phosphocholine 59, C_3H_9N), confirming the potassiated species of PC (36:2) (Supplementary Fig. S4). The MS/MS product ions of precursor ion *m/z* = 560.31128 confirm the potassium-attached monounsaturated LPC(18:1) (Supplementary Fig. S3).

3.2. Reproducibility of AP-SMALDI analysis of organ-specific lipid distributions

In order to discover and map the similarity and reproducibility of organ-specific lipid distributions, an MSI study was performed using representative biological replicates of female flies. Fig. 3 shows the characteristic spatial distribution of the ether-linked PC(O-36:2)/PC(P-36:1) in the head and antennal lobe of two biological replicates of adult female flies. The spatially resolved major abundant lipids that were found from head were ceramide phosphoethanolamines (Cer-PEs), ether lipids, and saturated PCs and PEs (Table 1). The Cer-PEs are membrane lipids that belong to the class of sphingolipids, having diverse functions in cellular and developmental processes. They are important regulators of *Drosophila* development and play a crucial role in brain development, phototransduction and behavior of the fruit fly [55–57]. Some of the most abundant lipids in the head are ether lipids. This is in clear agreement with a previous study on larval brain tissue and adult *D. melanogaster* brain [18,58].

The lipid distribution in *D.melanogaster* whole-body sections shows a unique profile with high levels of lysolipids, phosphatidylcholines and phosphatidylethanolamines. Lysolipids are phospholipase A (PLA)-type enzyme-catalyzed derivatives of phospholipids and are involved in important signaling functions as antimicrobial compounds [59]. The abundant expression of lysolipids (*m/z* = 400-600) throughout the whole fly reflects the high enzymatic activity in the animal [60,61]. Distribution of LPC(18:1) is shown for three whole-body sections of female flies in Fig. 3. The on-tissue MS/MS analysis of potassium-attached LPC(18:1) directly from the tissue confirmed its identity with respect to lipid class and overall composition of the hydrocarbon chain parts (Supplementary Fig. S3).

A high abundance of phosphatidylserines was detected specifically around the abdominal region from all replicates of the fly. Other phospholipids identified especially from the abdominal region are summarized in Table 1. The main digestion and nutrient absorption takes place in the metabolically active and permeable tissue of the gut, including uptake and processing of FAs. A unique distribution of arachidyl carnitine was identified from the abdominal region of the female fly within the mass accuracy of 0.55 ppm of potassium adducts

Table 2
Fatty acids and lipids detected in AP-SMALDI MSI analyses of male and female *Drosophila melanogaster* in negative-ion mode using pNA as a matrix. Structures were assigned based on accurate mass and database information from METLIN and LIPID MAPS.

Formula	Theoretical m/z $[M-H]^-$	Observed Mass $[M-H]^-$	Mass accuracy (ppm)	Theoretical m/z $[M+H]^+$	Observed Mass $[M+H]^+$	Mass accuracy (ppm)	Identity	Anatomy
$C_{12}H_{20}O_3$	211.13287	211.13316	1.36	213.14907	Not detected	Not detected	oxo-dodecenoic acid	Whole fly
$C_{14}H_{26}O_2$	225.18491	225.18542	2.31	227.20111	Not detected	Not detected	tetradecenoic acid C(14:1)	Whole fly
$C_{14}H_{28}O_2$	227.20055	227.20112	2.48	229.21675	Not detected	Not detected	tetradecanoic acid C(14:0)	Whole fly
$C_{14}H_{26}O_3$	241.17982	241.18025	1.79	243.19602	Not detected	Not detected	oxo-tetradecanoic acid	Whole fly
$C_{16}H_{28}O_2$	251.20055	251.20118	2.50	253.21675	Not detected	Not detected	hexadecadienoic acid	Whole fly
$C_{18}H_{30}O_2$	277.21621	277.21697	2.75	279.23241	Not detected	Not detected	octadecatrienoic acid C18:3	Head, Esophagous and Thorax
$C_{18}H_{32}O_2$	279.23185	279.23170	-0.54	281.24805	Not detected	Not detected	octadecadienoic acid C18:2	Whole fly
$C_{18}H_{34}O_2$	281.24751	281.24711	-1.39	283.26371	Not detected	Not detected	octadecenoic acid C18:1	Whole fly
$C_{18}H_{32}O_3$	295.22677	295.22762	2.89	297.24297	Not detected	Not detected	hydroxy-octadecadienoic acid C18:2(OH)	Whole fly
$C_{18}H_{34}O_3$	297.24242	297.24334	3.09	299.25862	Not detected	Not detected	hydroxy-octadecenoic acid C18:1(OH)	Whole fly
$C_{18}H_{32}O_4$	311.22169	311.22074	3.05	313.23789	Not detected	Not detected	dihydroxy-octadecadienoic acid	Head and Thorax
$C_{21}H_{44}NO_7P$	452.27717	452.27742	0.57	454.29282	454.29252	−0.63	LPE(16:0)	Whole fly
$C_{23}H_{46}NO_7P$	478.29282	478.29298	0.34	480.30847	480.30864	0.37	LPE(18:1)	Whole fly
$C_{23}H_{48}NO_7P$	480.30847	480.30864	0.37	482.32412	482.32450	0.78	LPE(18:0)	Head, Esophagous and Gut
$C_{22}H_{45}O_9P$	483.27175	483.27291	2.40	485.28740	Not detected	Not detected	LPG(16:0)	Whole fly
$C_{25}H_{44}NO_7P$	500.27717	500.27693	-0.48	502.29282	502.29302	0.40	LPE(20:4)	Whole fly
$C_{25}H_{52}NO_7P$	508.33977	508.34082	2.07	510.35597	510.35738	2.76	LPE(20:0)	Head, Esophagous and Gut
$C_{24}H_{47}O_9P$	509.28740	509.28847	2.11	511.30360	Not detected	Not detected	LPG(18:1)	Whole fly
$C_{24}H_{46}NO_9P$	522.28264	522.28381	2.25	524.29829	524.29924	1.80	LPS(18:1)	Whole fly
$C_{26}H_{45}O_9P$	531.27175	531.27263	1.67	533.28740	Not detected	Not detected	LPG(20:4)	Whole fly
$C_{28}H_{56}NO_7P$	548.37107	548.37163	1.02	550.38727	550.38835	1.96	PC-O(20:1)	Head and Esophagous
$C_{28}H_{45}O_9P$	555.27175	555.27220	0.81	557.28740	Not detected	Not detected	LPG(22:6)	Whole fly
$C_{29}H_{58}NO_7P$	562.38725	562.38809	1.49	564.40345	564.40263	−1.44	LPE(24:1)	Head and Esophagous
$C_{30}H_{55}O_9P$	589.35000	589.35176	2.99	591.36620	Not detected	Not detected	LPG(24:3)	Whole fly
$C_{30}H_{59}O_9P$	593.38130	593.38117	-0.22	595.39750	Not detected	Not detected	LPG(24:1)	Head and Esophagous
$C_{27}H_{53}O_{12}P$	599.31909	599.31833	-1.27	601.33474	Not detected	Not detected	LPI(18:0)	Head, Esophagous and Gut
$C_{30}H_{54}NO_9P$	602.34525	602.34709	3.07	604.36145	Not detected	Not detected	LPS(24:3)	Whole fly
$C_{30}H_{56}NO_9P$	604.36090	604.36172	1.37	606.37710	Not detected	Not detected	LPS(24:2)	Whole fly
$C_{30}H_{58}NO_9P$	606.37655	606.37842	3.10	608.39275	608.39437	2.66	LPS(24:1)	Whole fly
$C_{30}H_{57}O_{10}P$	607.36056	607.36155	3.29	609.37676	Not detected	Not detected	PG(24:1)	Whole fly
$C_{33}H_{58}NO_7P$	610.38672	610.38694	0.37	612.40292	612.40258	−0.54	LPE(28:5)	Gut region
$C_{33}H_{60}NO_7P$	612.40237	612.40258	0.36	614.41857	Not detected	Not detected	LPE(28:4)	Gut region
$C_{32}H_{57}O_9P$	615.36565	615.36713	2.42	617.38185	Not detected	Not detected	LPG(26:4)	Whole fly
$C_{33}H_{61}O_8P$	615.40203	615.40373	2.77	617.41823	617.41976	2.47	PA(30:2)	Gut region
$C_{29}H_{49}O_{12}P$	619.28779	619.28817	0.62	621.30344	621.30422	1.25	LPI(20:4)	Whole fly
$C_{30}H_{56}NO_{10}P$	620.35581	620.35734	2.48	622.37201	622.37309	1.73	PS(24:1)	Whole fly
$C_{32}H_{64}NO_8P$	620.42858	620.42825	-0.54	622.44478	622.44549	1.13	PC(24:0)	Head and Esophagous
$C_{30}H_{58}NO_{10}P$	622.37146	622.37309	2.63	624.38766	624.38724	−0.67	PS(24:0)	Whole fly
$C_{32}H_{58}NO_9P$	630.37655	630.37828	2.76	632.39275	632.39402	2.00	LPS(26:3)	Whole fly
$C_{32}H_{60}NO_9P$	632.39220	632.39402	2.89	634.40840	634.40973	2.10	LPS(26:2)	Whole fly
$C_{32}H_{62}NO_9P$	634.40785	634.40973	2.98	636.42405	636.42538	2.08	LPS(26:1)	Whole fly
$C_{32}H_{64}NO_9P$	636.42350	636.42538	2.96	638.43970	638.44061	1.43	LPS(26:0)	Head and Esophagous
$C_{35}H_{64}NO_7P$	640.43367	640.43423	0.89	642.44987	Not detected	Not detected	LPE(30:4)	Gut region
$C_{35}H_{65}O_8P$	643.43333	643.43524	2.97	645.44953	645.45097	2.23	PA(32:2)	Whole fly
$C_{35}H_{67}O_8P$	645.44898	645.45097	3.10	647.46518	647.46672	2.38	PA(32:1)	Whole fly
$C_{34}H_{66}NO_8P$	646.44423	646.44508	1.32	648.46043	648.46091	0.73	PC(26:1)	Head,Esophagous and Gut
$C_{32}H_{60}NO_{10}P$	648.38711	648.38902	2.95	650.40331	650.40409	1.19	PS(26:1)	Whole fly
$C_{34}H_{68}NO_8P$	648.45988	648.45891	-1.51	650.47608	650.47668	0.91	PC(26:0)	Head and Esophagous
$C_{38}H_{77}N_2O_6P$	687.54355	687.54552	2.88	689.55975	689.56015	0.58	Cer-PE (36:1)	Head and Esophagous
$C_{37}H_{72}NO_8P$	688.49118	688.49313	2.83	690.50738	690.50933	2.82	PE(32:1)	Whole fly
$C_{39}H_{75}O_8P$	701.51158	701.51217	0.84	703.52723	703.52825	1.44	PA(36:1)	Gut region
$C_{39}H_{74}NO_8P$	714.50683	714.50781	1.38	716.52303	716.52495	2.67	PE(34:2)	Whole fly
$C_{39}H_{76}NO_8P$	716.52248	716.52295	0.66	718.53868	718.53807	−0.85	PE(34:1)	Whole fly
$C_{39}H_{78}NO_8P$	718.53813	718.53838	0.36	720.55378	720.55315	−0.87	PE(34:0)	Head, Esophagous and Gut
$C_{38}H_{75}O_{10}P$	721.50141	721.50338	2.74	723.51706	Not detected	Not detected	PG(32:0)	Gut region
$C_{41}H_{74}NO_8P$	738.50683	738.50662	-0.30	740.52303	740.52468	2.22	PE(36:4)	Whole fly
$C_{41}H_{78}NO_8P$	742.53813	742.53856	0.59	744.55378	744.55330	−0.65	PE(36:2)	Whole fly
$C_{40}H_{76}NO_{10}P$	760.51231	760.51427	2.58	762.52796	762.52842	0.60	PS(34:1)	Gut region

(continued on next page)

Table 2 *(continued)*

Formula	Theoretical m/z $[M-H]^-$	Observed Mass $[M-H]^-$	Mass accuracy (ppm)	Theoretical m/z $[M+H]^+$	Observed Mass $[M+H]^+$	Mass accuracy (ppm)	Identity	Anatomy
$C_{42}H_{75}O_{10}P$	769.50141	769.50213	0.94	771.51706	Not detected	Not detected	PG(36:4)	Head, Esophagous and Thorax
$C_{42}H_{81}O_{10}P$	775.54836	775.55050	2.77	777.56401	Not detected	Not detected	PG(36:1)	Gut region
$C_{42}H_{74}NO_{10}P$	782.49666	782.49622	-0.57	784.51231	784.51368	1.75	PS(36:4)	Whole fly
$C_{42}H_{80}NO_{10}P$	788.54361	788.54560	2.53	790.55926	790.55994	0.85	PS(36:1)	Head, Esophagous and Gut
$C_{41}H_{75}O_{13}P$	805.48616	805.48774	3.21	807.50236	807.50476	2.97	PI(32:2)	whole fly
$C_{46}H_{79}O_9P$	805.53780	805.53703	-0.95	807.55400	Not detected	Not detected	PG(P-40:6)	Head and Esophagous
$C_{41}H_{77}O_{13}P$	807.50181	807.50275	3.65	809.51801	Not detected	Not detected	PI(32:1)	Whole fly
$C_{41}H_{79}O_{13}P$	809.51746	809.51971	2.78	811.53311	Not detected	Not detected	PI(32:0)	Whole fly
$C_{44}H_{78}NO_{10}P$	810.52796	810.52666	-1.61	812.54361	812.54331	−0.37	PS(38:4)	Whole fly
$C_{43}H_{75}O_{13}P$	829.48616	829.48845	2.76	831.50236	831.50430	2.33	PI(34:4)	Whole fly
$C_{43}H_{77}O_{13}P$	831.50181	831.50430	2.99	833.51801	833.52004	2.44	PI(34:3)	Whole fly
$C_{43}H_{79}O_{13}P$	833.51746	833.51804	0.70	835.53366	Not detected	Not detected	PI(34:2)	Whole fly
$C_{43}H_{81}O_{13}P$	835.53311	835.53326	3.77	837.54876	Not detected	Not detected	PI(34:1)	Whole fly
$C_{43}H_{83}O_{13}P$	837.54876	837.55044	3.21	839.56441	839.56672	2.75	PI(34:0)	Whole fly
$C_{45}H_{75}O_{13}P$	853.48616	853.48673	0.67	855.50236	Not detected	Not detected	PI(36:6)	Head and Esophagous
$C_{48}H_{74}NO_{10}P$	854.49666	854.49548	-1.38	856.51286	Not detected	Not detected	PS(42:10)	Gut region
$C_{45}H_{77}O_{13}P$	855.50181	855.50380	2.33	857.51801	Not detected	Not detected	PI(36:5)	Whole fly
$C_{48}H_{92}NO_9P$	856.64260	856.64447	2.19	858.65880	Not detected	Not detected	PS(P-42:1)	Gut region
$C_{45}H_{79}O_{13}P$	857.51746	857.51844	1.15	859.53366	859.53516	1.74	PI(36:4)	Whole fly
$C_{48}H_{91}O_{10}P$	857.62661	857.62683	0.25	859.64281	Not detected	Not detected	PG(42:2)	Gut region
$C_{45}H_{81}O_{13}P$	859.53311	859.53416	1.22	861.54931	861.55023	1.07	PI(36:3)	Whole fly
$C_{45}H_{83}O_{13}P$	861.54876	861.55123	2.87	863.56441	Not detected	Not detected	PI(36:2)	Whole fly
$C_{45}H_{85}O_{13}P$	863.56441	863.56540	1.15	865.58006	865.57825	−2.08	PI(36:1)	Gut region
$C_{45}H_{87}O_{13}P$	865.58006	865.57825	-2.09	867.59571	867.59627	0.65	PI(36:0)	Gut region
$C_{48}H_{90}NO_{10}P$	870.62186	870.62371	2.12	872.63806	872.63891	0.97	PS(42:2)	Gut region
$C_{45}H_{86}NO_{13}P$	878.57531	878.57455	-0.86	880.59151	Not detected	Not detected	PI(36:2)	Whole fly
$C_{47}H_{79}O_{13}P$	881.51746	881.51733	-0.15	883.53311	883.53249	−0.69	PI(38:6)	Whole fly
$C_{47}H_{81}O_{13}P$	883.53311	883.53249	-0.70	885.54876	885.54865	−0.11	PI(38:5)	Whole fly
$C_{47}H_{87}O_{13}P$	889.58006	889.58100	1.06	891.59626	Not detected	Not detected	PI(38:2)	Gut region
$C_{47}H_{89}O_{13}P$	891.59571	891.59735 92 deprotonated lipids	1.84	893.61191	Not detected 48 lipids in both positive and negative mode	Not detected	PI(38:1)	Gut region

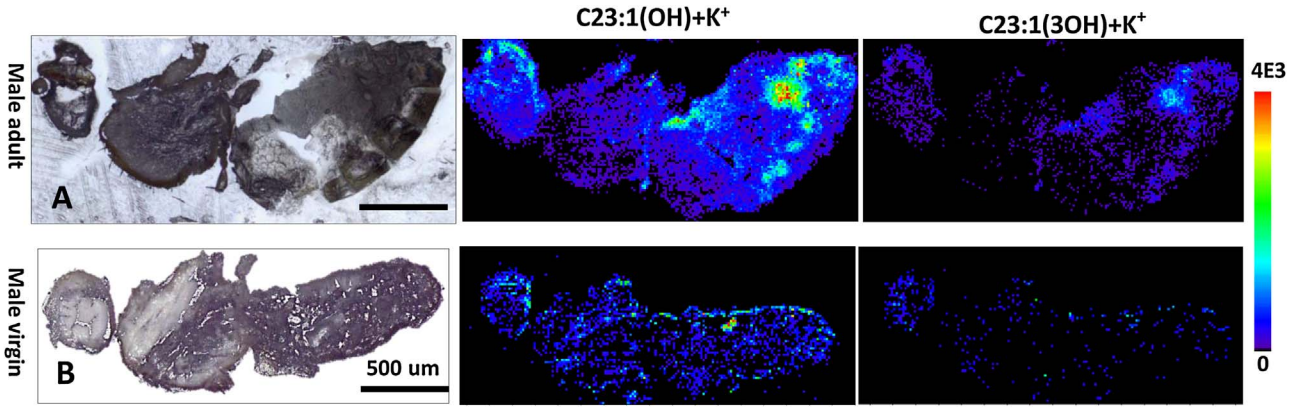

Fig. 7. Distribution of male-specific potassium-attached pheromones C23:1(OH) (m/z = 377.3201) and C23:1(3OH) (m/z = 409.3100 within 5 ppm mass accuracy) in A) mated and B) virgin male *D. melanogaster*. Higher intensities of these pheromones were observed around the genital region of mated flies compared to the virgin flies, which show lower intensities and a more homogeneous distribution of the pheromones throughout the body. Images were generated with 15 μm per pixel. AP-SMALDI image sizes were 192 × 96 pixels and 154 × 78 pixels, respectively). The scale bar represents 500 μm.

species (Fig. 3 and Table 1). Carnitines are reported as an essential nutrient for insects and are involved in the transport of free FA into and out of the mitochondria [60,62].

All lipids were imaged based to the three most prominent ion species, as mentioned earlier, and each image of the lipids was scaled from the lowest (black) to highest (red) intensity. The distributions of lipids can be determined reproducibly, although they vary to some extent, due to the heterogeneity of the different biological replicates. Sample preparation for reproducible imaging is challenging, including tissue sectioning and matrix application. In addition, reproducible laser focusing in consecutive measurements is also of paramount importance.

The MS images of lipids were generated using an m/z bin width of

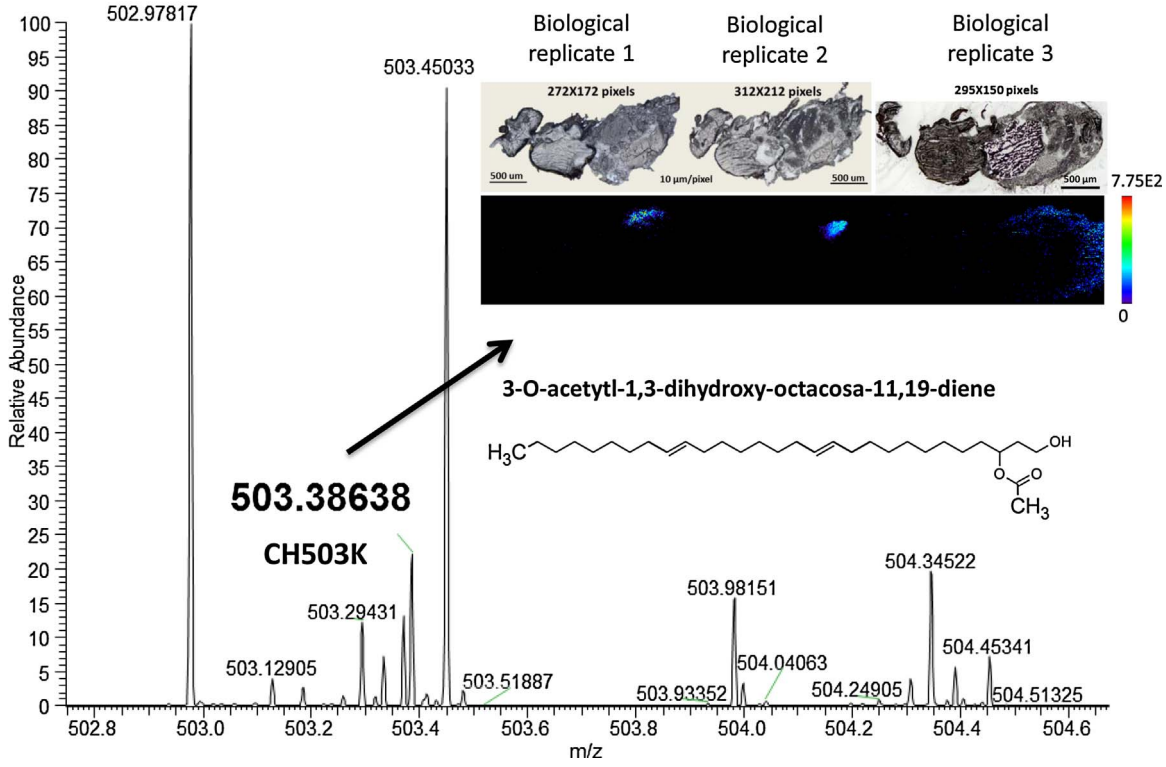

Fig. 8. AP-SMALDI MSI of sections from three adult female mated biological replicates of *D. melanogaster*, revealing the transferred male-specific pheromone CH503 (potassium attached *m/z* 503.38638, 0.55 ppm) in the female genital region or reproductive tract. The displayed mass spectrum was averaged from 1521 pixels within the genital region. In each measurement the resolution was set to 10 µm per pixel (10 µm step size).

0.01 u or ± 5 ppm relative to the exact mass values of the three ion species of the lipids. All potassiated species of lipids assigned with a mass accuracy of better than ± 1 ppm both from adult male and female *D. melanogaster* are summarized in Table 1.

3.3. AP-SMALDI imaging in negative ion mode

Two adjacent 20 µm sections of female *D. melanogaster* were measured to identify lipids and examine the reproducibility after pNA application at a lateral resolution of 8 µm/pixel. A total of 89 deprotonated lipids were identified in negative-ion mode within the mass range of *m/z* = 200-900, among them 14 lipids identified as FAs. Six classes of phospholipids and lysophospholipids were identified in the form of phosphatidylcholines (PCs), phosphatidylethanolamines (PEs), phosphatidic acids (PAs), phosphatidylglycerols (PGs), phosphatidylserines (PSs), and phosphatidylinositols (PIs). The majority of the lipids identified in negative-ion mode MSI were PIs, followed by PSs, PEs, PGs, PAs, and, in a much lower amount, PCs. Some of the lipids structurally assigned by accurate mass, were subsequently identified by on-tissue MS/MS analysis. A few examples of those are shown with their MS/MS spectra in Supplementary Figs. S5–S7, acquired using pNA as a matrix in negative-ion mode.

Only a few sphingolipids could be identified in negative-ion mode in the form of deprotonated lipids, mainly sphingolipid Cer-PE(36:1) in the head. Most lipids identified using pNA as a matrix in negative-ion mode were not found as DHB-ionized lipids in positive-ion mode, except for LPE (16:1), Cer-PE(36:1) and PEs (32:1, 34:2, 36:2), which were identified with both matrices and ion polarities. A typical RGB image of three selected lipid signals is shown in Fig. 4, where the red pixel distribution in head of three adjacent female-fly sections corresponds to ether PC(O-20:1)/PC(P-20:0) (*m/z* 548.37163), and the green image describes the distribution of abundant PI(34:2) (*m/z* 833.51804) in the whole body. A lysophosphatidylethanolamine, LPE(28:4) (*m/z* 612.40258) observed to be distributed around the cuticle of the gut region of three adjacent sections of the fly, shown as a blue pixel distribution. These three ion images were combined into one RGB image in order to depict their anatomical distributions in parallel (Fig. 4). Fatty acids have important roles in mammals, including reproduction, cold adaptation and metabolism [63].

It has been suggested that the presence and composition of FAs in cell membranes affect cold adaptation and cell signaling in *D. melanogaster*, especially by C18 FAs [63–65]. Moreover, a change of the FA content can affect female fecundity, remating and production of sex hormones [66,67]. Three C18 FAs and their anatomical distributions are shown in Fig. 5 with FA(C18:3) depicted in red, FA(C18:2) in green and FA(C18:1) in blue, along with an RGB overlay of those selected FAs. Fatty acids with 18 carbon atoms were found in the whole body of the fruit fly. On-tissue MS/MS fragmentation of possible FA(18:2), is shown in Supplementary Fig. S5. Another adjacent section of the same female fly was used to characterize the protonated lipids in positive-ion mode in comparison to the deprotonated lipids, expectedly showing a similar spatial distribution. A total of 48 lipids were identified in both positive- and negative-ion mode, all expressing a similar spatial distribution. Similarity in distribution patterns of positive and negative ion species for two adjacent sections is shown in Supplementary Fig. S11 for PE (34:1), LPE(18:0), LPS(18:1), and Cer-PE(36:1). Using AP-SMALDI MSI, the anatomical distribution of lipids, such as PE(36:2), was not only explored with high mass accuracy in protonated and deprotonated

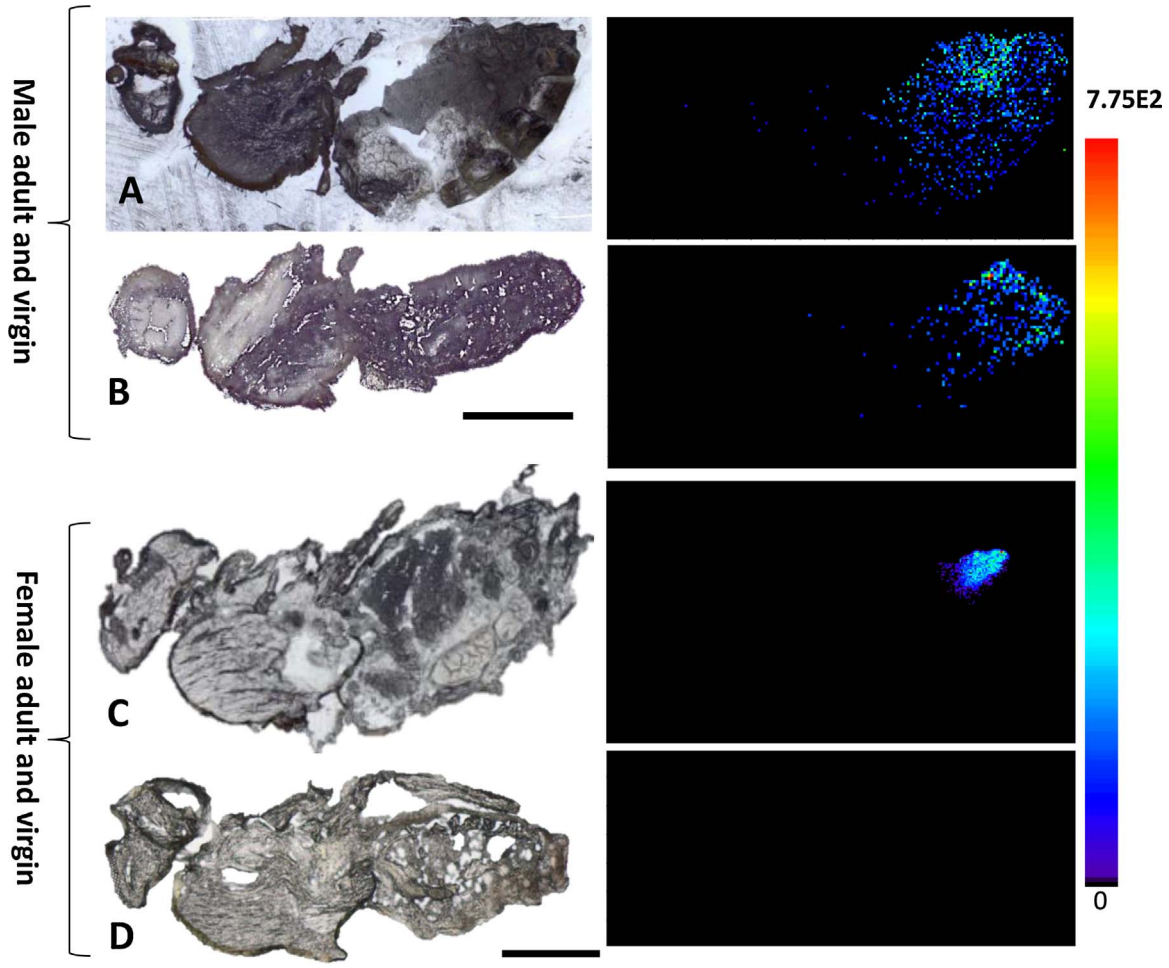

Fig. 9. AP-SMALDI MSI of the male sex pheromone CH503 in sections of A) adult mated male (image of 192 × 96 pixels, generated at 15 µm per pixel) and of B) virgin male *D. melanogaster* (image of 154 × 78 pixels, generated at 15 µm per pixel), exhibiting a diffuse distribution within the posterior of the flies. C) The male pheromone was also found in the genital region of mated female flies supposedly transferred from the male fly during mating. The measurement was performed at 10 µm per pixel for 312 × 212 pixels. D) CH503 was not found in virgin female flies. The size of the measurement was 164 × 70 pixels and the step size was 15 µm per pixel.

mode, but compounds were also identified by MS/MS directly from another neighboring section (Fig. 6). We detected the characteristic neutral loss from the head group of protonated PE(36:2) in positive-ion mode, whereas characteristic loss of hydrocarbon chain from the precursor ion of PE(36:2) was recorded in negative-ion mode. Similar images of the lipid precursor ions in positive- and negative-ion mode from adjacent sections are shown in Fig. 6. Future work will focus on the quantification of lipids directly from tissue and the differentiation of isomers. All detected lipids, measured with pNA as a matrix and assigned within a mass accuracy of ± 3 ppm are summarized in Table 2.

3.4. AP-SMALDI imaging of pheromones

The high resolution and sensitivity of our instrumentation enabled characterization of oxygen-containing putative pheromones both from mated and virgin male and female flies with precise visualization, localization and high mass accuracy and, furthermore, allowed the differentiation between sexes of the biological replicates. Insect pheromones i.e cuticular hydrocarbons (CHCs) had been analyzed previously by conventional GC/MS [68] after organic-solvent extraction. Although GC/MS allows the structural characterization of volatile nonpolar hydrocarbons, such as alkanes and alkenes, it is not usable to elucidate the spatial information of larger or more polar compounds because of the extraction procedure [69]. On the other hand, non-conventional direct ultraviolet laser desorption/ionization orthogonal time-of-flight MS (UV-LDI-o-TOF MS) was applied to desorb molecules from the cuticular surface by using a 200 µm-diameter laser beam that enabled a spatial chemical profiling of 28 species of CHCs [16]. This technique expands the detection range of polar compounds from the cuticular anatomy of the fruit flies, but does not provide highly resolved topological localization and distributional images from the anatomical sections. Mass spectrometry imaging of two lipophilic putative male sex pheromones has recently been introduced [10], using a Synapt G2-S HDMS (Waters/Micromass, Manchester, UK) hybrid orthogonal TOF MS containing a modified ion source [10]. However, mass resolution of that instrumentation was not high enough to obtain the accurate mass of typical lipophilic pheromones, as for example the acetylated male-specific polar hydrocarbon named CH503 (3R, 11Z, 19Z)-3-acetoxy-11, 19-octacosadien-1-ol. The latter is highly abundant in the male genital region of *D. melanogaster* and is transferred to the female genital integument during copulation and inhibits the male courtship behavior [10,16].

In order to explore the distinct distribution patterns of pheromones within whole-body sections of the fly based on accurate mass, we employed high-resolution AP-SMALDI MSI in positive-ion mode by

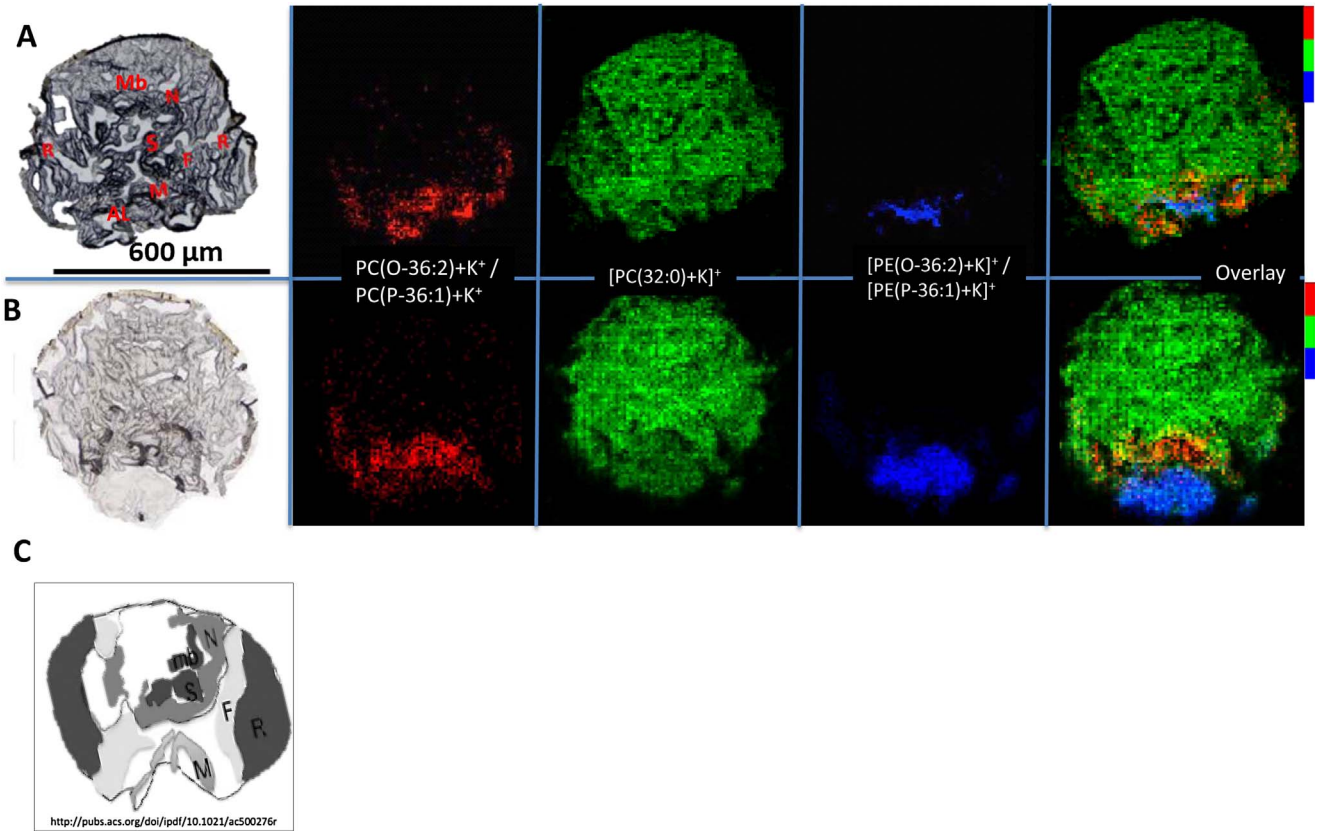

Fig. 10. AP-SMALDI MSI of head sections from two biological replicates (A and B) of *D. melanogaster*, showing three brain-specific lipids ($[M+K]^+$ signals of phosphatidylcholines PC(O-36:2)/PC(*P*-36:1), m/z 810.57799, 0.80 ppm, PC(32:0), m/z 772.52511, −0.26 ppm and PE(O-36:2)/PE(P-36:1), m/z 766.51475, −0.49 ppm) measured in positive-ion mode with 10 µm per step. Image sizes were 116 × 116 pixels and 122 × 110 pixels, respectively. The lipids show reproducible distributions in the various parts of the fly brain. Imaging bin width was $\Delta m/z$ = 0.01 at a mass resolving power of 140,000 at m/z 200 and a mass accuracy of better than 3 ppm. The RGB overlay images of the three selected lipid species are shown to the right. C) Abbreviations for the various locations in the cartoon sketch image are as follows: R = retina (without pigment), F = fat bodies, M = mouthparts, N = cortex with nuclei, S = synaptic neurons, Mb = mushroom bodies, AL = antennal lobe. (Adapted from [58]).

using DHB as a matrix. Spatial distribution, characterization and differentiation of male- and female-specific polar cuticular hydrocarbons or putative pheromones were studied based on high resolution in mass and space, but, due to volatility of some pheromones and heterogeneity of the tissue, a discrete pattern of compound distribution was difficult to obtain. A mass spectrum averaged from 618 spots from the genital region of the adult male fly is shown in Supplementary Fig. S12, depicting three lipophilic putative male pheromones within the mass range of m/z = 300–600. Signals correspond to the singly charged potassium-attached hydroxylated hydrocarbons C23:1(OH) ($C_{23}H_{46}O$), C23:1(3OH) ($C_{23}H_{46}O_3$) and C30:2(OAc + OH) ("CH503" = $C_{30}H_{56}O_3$), assigned within the mass accuracy of ± 1 ppm according to Y. Shikichi et al. [70]. The detected pheromones C23:1(OH) and C23(3OH) were found to be distributed all over the body of adult and mated male and virgin male flies, but the concentration was found to be higher within the anogenital region of the adult mated male after copulation compared to virgin male flies (Fig. 7). These male pheromones have a great influence on communication cues and courtship behavior, since initial suppression of male courtship is partially mediated by the transfer of these pheromones to females [10,16].

We identified CH503 in 20 µm sections of adult mated females from three biological replicates with a distinct location of the male sex pheromone in the female genital integument region (Fig. 8). Visualization of the male-specific sex pheromone CH503 within mated versus virgin *D. melanogaster* revealed a similar distribution pattern, diffusely located around the genital region of both, mated adult and virgin male flies (Fig. 9).

This observation is in accordance with the supposed transfer of this sex pheromone from the male to the female during mating [16]. We performed further studies to compare virgin female flies with mated female flies, as well as virgin and mated male flies, and we found a clear indication of CH503 after copulation in both sexes (Fig. 9). In summary, this recent MSI study provides a highly resolved visualization of the distinct localization and distribution of these characteristic pheromones in male and female *D. melanogaster*. It has to be noted that high mass resolution and mass accuracy were necessary in these MSI studies to discriminate the pheromones from closely neighboring mass signals of other compounds (see Figs. 10A and 11A).

3.5. Molecular imaging of Drosophila brain

High-resolution AP-SMALDI imaging of *D. melanogaster* brains explored the topographic distribution of lipids, metabolites and neuropeptides in different parts, including the retina, fat bodies, mouth parts, cortex, synaptic neurons, mushroom bodies, and antennal lobe from the coronal sections [58]. The dissected *D. melanogaster* head was embedded in 5% gelatin and carefully sliced into 20 µm thick sections with our cryo-microtome from the dorsal to the caudal area in order to maintain the intact morphology of the fly brain, which is smaller than

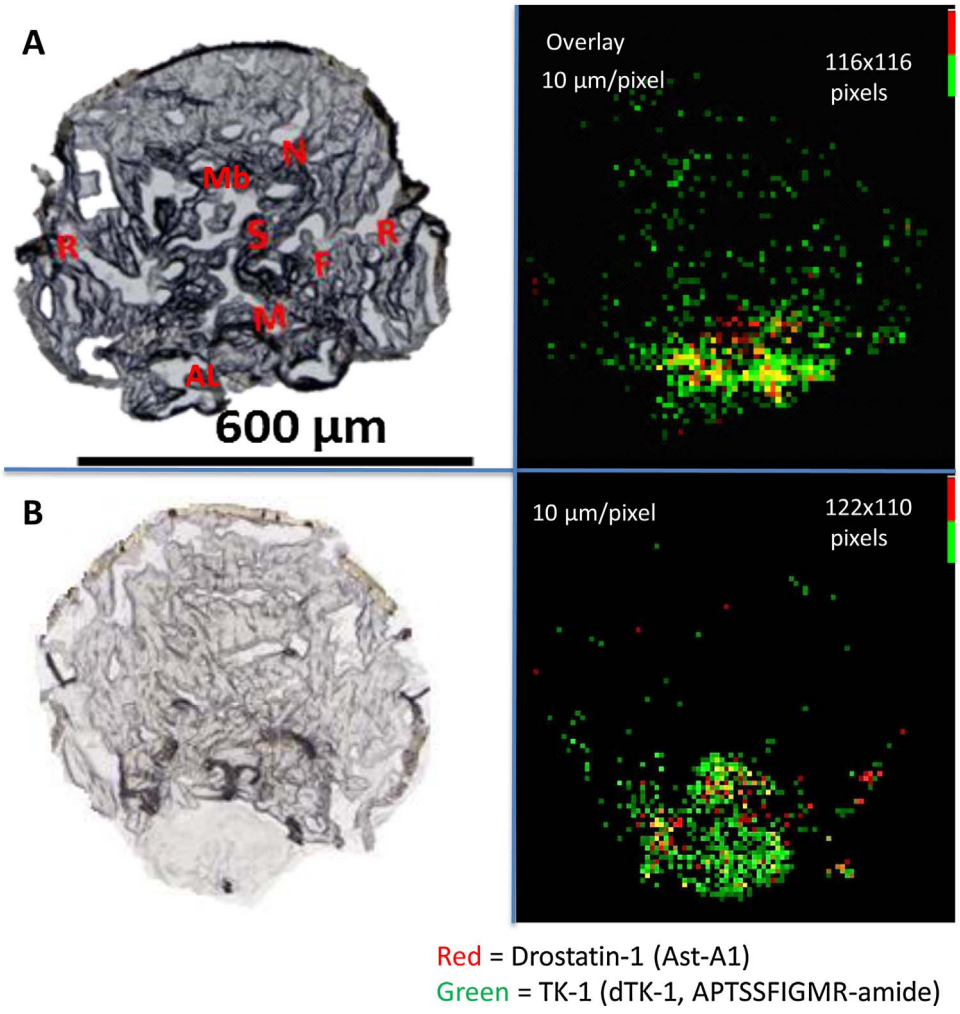

Fig. 11. AP-SMALDI MSI of sections from the heads of two biological replicates (A and B) of *D. melanogaster*, indicating the distribution of two protonated peptides drostatin-1 (*m/z* 953.52118, 2.0 ppm) and TK-1 (*m/z* 1065.54895, 2.01 ppm), overlaid in red and green. Measurements were performed with 10 µm per pixel in positive-ion mode, using DHB as a matrix. (For interpretation of the references to colour in this figure legend, the reader is referred to the web version of this article.)

1 mm in diameter (Supplementary Fig. S13). The optical images of the sections were later compared to the MSI-measured sections which were subsequently stained with hematoxylin and eosin (H & E) to determine anatomical correlations between mass spectrometric and histological data. Anatomical correlations between microscopic image, mass spectrometric image and an H & E-stained optical image are shown in Supplementary Fig. S13. The unique distributions of eight brain-specific lipids were determined from the two biological replicates of fly brain, measured with 10 µm/pixel resolution. A high similarity was found for the lipid distributions in the two replicates, confirming the high degree of reproducibility of lipid topography and MSI methodology (Fig. 10 and Table 1).

High-resolution AP-SMALDI MSI using DHB as a matrix in positive-ion mode also enabled us to identify 14 spatially resolved *D. melanogaster* neuropeptides within the *m/z* range of 900–1100 and a mass accuracy of ± 3 ppm (Table 3). All neuropeptides were assigned based on accurate mass and on identifications described in other studies of *D. melanogaster*. [33]. Nine of those were allatostatins and tachykinin-like peptides. Allatostatins are the major group of insect neuropeptides, acting on central parts of the fly brain in order to block the release of juvenile hormones and on the gut to block smooth muscle contraction and motoneuron modulation [71]. On the other hand, tachykinin-like peptides (TKLPs) are common in both vertebrates and invertebrates. This family of neuropeptides regulates the function of odor perception and locomotor activity in *D. melanogaster* [72]. Other neuropeptides identified here include FMRFamide (Phe-Met-Arg-Phe)-related peptides, which have functions in muscle contractions at neuromuscular junctions in the fruit fly [73]. Short NPF-like peptides were found to be concentrated in the mushroom bodies of the fly brain, an area which is involved in learning and memory [74]. These peptides have functions in various physiological processes and are expressed during all developmental stages of *D. melanogaster*. AP-SMALDI averaged mass spectra show one of the allatostatin peptides (drostatin-1, red) and tachykinin-like peptides (TK-1, green) in Supplementary Fig. S14. The localization of these two peptides in head sections of two biological replicates of *D. melanogaster* is shown in Fig. 11.

High-resolution AP-SMALDI MSI at a spatial resolution of 5 µm/pixel from the upper part of a coronal section of female *D. melanogaster* head allowed the identification of 19 different metabolites within the mass accuracy of ± 2 ppm and in the mass range of *m/z* = 80–400 (Table 4). The metabolomic profile of *D. melanogaster* has been discussed previously by Kamleh et al., who used liquid chromatography

Table 3
Neuropeptides detected in AP-SMALDI MSI analyses of the head of *Drosophila melanogaster* in positive-ion mode using DHB as a matrix. Structures were assigned based on accurate mass and literature data.

Formula	[M]mono	$[M+H]^+_{calc}$	Observed *m/z*,[M + H] $^+$	Mass error/ ppm	$[M+K]^+$	Observed *m/z*,[M + K] $^+$	Mass error/ ppm	$[M+Na]^+$	Observed *m/z*,[M + Na] $^+$	Mass error/ppm	Peptide name	Peptide sequence
$C_{43}H_{64}N_{12}O_{11}$	924.48175	925.48958	925.49143	2.0	963.44491	n.d	n.d	947.47097	n.d	n.d	Drostatin-3 (Ast-A3)	R.SRPYSFGLa.G
$C_{40}H_{65}N_{13}O_{11}S_1$	935.46472	936.47255	936.47522	2.8	974.42788	n.d	n.d	958.45394	n.d	n.d	TK-3 (dTK-3, APTGFTGMRamide)	R.APTGFTGMRa.G
$C_{45}H_{75}N_{13}O_9$	941.58107	942.58890	942.58316	nd	980.54423	980.54514	0.92	964.57029	n.d	n.d	TK-2 (dTK-2, APLAFVGLRamide)	K.APLAFVGLRa.G
$C_{45}H_{68}N_{12}O_{11}$	952.51305	953.52088	953.52275	2.0	991.47621	n.d	n.d	975.50227	975.50168	−0.61	Drostatin-1 (Ast-A1)	R.VERYAFGLa.G
$C_{42}H_{68}N_{14}O_{10}S_1$	960.49636	961.50418	961.50321	−1.0	999.45952	n.d	n.d	983.48557	n.d	n.d	TK-5 (dTK-5, APNGFLGMRamide	R.APNGFLGMRa.G
$C_{45}H_{75}N_{17}O_8$	981.59845	982.60628	n.d	n.d	1020.56161	1020.55296	n.d	1004.58760	1004.58581	−1.857910474	sNPF-3 (KPQRLRWamide)	R.KPQRLRWa.G
$C_{45}H_{76}N_{16}O_7S_1$	984.58036	985.58819	985.58659	−1.6	1023.54352	n.d	n.d	1007.56958	n.d	n.d	sNPF-4 (KPMRLRWamide)	R.KPMRLRWa.G
$C_{44}H_{75}N_{15}O_{10}$	973.58214	974.58996	n.d	n.d	1012.54529	1012.54485	−0.43	996.57135	n.d	n.d	RLRF peptide 2	R.SPSLRLRFa.G
$C_{46}H_{76}N_{14}O_{13}S_1$	1064.54370	1065.55153	1065.54932	−2.018	1103.50686	1103.50841	1.4	1087.53292	n.d	n.d	TK-1 (dTK-1, APTSSFIGMRamide)	R.APTSSFIGMRa.G
$C_{47}H_{77}N_{15}O_{12}S_1$	1075.55969	1076.56751	1076.57437	nd	1114.52285	n.d	nd	1098.54890	1098.54733	−1.43	TK-4 (dTK-4, APVNSFVGMRamide)	R.APVNSFVGMRa.G
$C_{59}H_{89}N_{17}O_{15}$	1275.67241	1276.68023	n.d	nd	1314.63557	1314.63560	0.02753	1298.66162	n.d	n.d	Drostatin-4 (Ast-A4)	R.DQWQKLHGGWa.G
$C_{52}H_{79}N_{15}O_{13}S_1$	1153.56970	1154.57753	1154.57783	0.26	1192.53341	n.d	n.d	1176.559473	n.d	n.d	FMRFamide	R.TTRPQPFNFGLa.G
$C_{47}H_{62}N_8O_{16}$	994.42783	995.43621	995.43621	−1.43	1033.39099	nd	n.d	1017.417603	1017.41959	1.95	AST-1	R.SPKQDFMRFa.G
$C_{44}H_{72}N_{18}O_9S_2$	1060.51656	1061.52494	1061.52494	1.68	1099.47972	1099.48345	3.39031	1083.506332	nd	nd	AmTRP-5	A.YRKPPFNGSIFa.G

*nd = not detected.
*Reference: Salisbury JP, Boggio KJ, Hsu Y-WA, Quijada J, Sivachenko A, Gloeckner G, Kowalski PJ, Easterling ML, Rosbash M, Agar JN. Molecular Brain 2013, 6(1):1–15.

coupled to Fourier transform MS from insect homogenates [75]. In our study, the anatomical localization of small metabolites in different parts of the fly brain was discussed for the first time.

The identification and distribution pattern of the protonated small metabolites spermine (*m/z* 203.22285 polyamine, red, −0.84 ppm), clavepictine B (*m/z* 306.27865 sphingolipid, green, −1.60 ppm) and one of the four nucleobases, guanine (*m/z* 152.05660, blue, −0.56 ppm), is depicted in Fig. 12, showing a distinct topological distribution of these metabolites assigned to specific brain regions. MSI was performed at a resolution of 5 μm/pixel and the images obtained were overlaid in an RGB image in order to visualize their distributions in parallel. Polyamines can be found in species from bacteria to plants, insects and other animals. They have many important roles in biological systems including cell growth and cell proliferation [76] and act as functional markers of neoplasia [77]. They are linked to several diseases, including brain tumors [76], leukemia, cystic fibrosis, sickle cell anemia, and psoriasis [78]. Furthermore, polyamines are involved in heart and muscle hypertrophy [67]. Alkaloid properties of clavepictine B are actively involved in antimicrobial, antifungal and antitumor activity [78].

Three other metabolites and their overlay image are depicted in Fig. 12, including kynurenine (*m/z* 209.09188, red, −0.90 ppm) in the rostral part, tetradecadienyl histidine (histidine lipid, *m/z* 364.25982, green, 0.96 ppm), intensely found within the central part, and guanosine monophosphate (*m/z* 284.09865, GMP, blue, −1.04 ppm), which clusters around the caudal area of the fly brain. Kynurenines are involved in the pathology of neurodegenerative disorders, pain syndromes and autoimmune diseases [79]. The central part of the fly brain is concentrated with the distribution of tetradecadienyl histidine, consistent with a previous study of *Drosophila* metabolites [75]. All metabolites were assigned according to literature data [75] within the mass accuracy of ± 2 ppm (Table 4).

4. Conclusion

This high-resolution MSI study provided a visualization of lipids, metabolites, pheromones, and neuropeptides of *D. melanogaster* with an emphasis on their tissue-specific spatial distributions and intensities. Moreover, distribution and intensity changes of male-specific lipid-based pheromones within adult and virgin male and female flies were visualized, which would not have been disclosed with spatially low-resolving imaging instrumentation. Apart from this, a convenient method to prepare tissue sections for MSI studies of small and delicate insects is proposed that preserves the integrity and morphological features of the fly after embedding in 5% CMC or in gelatin in the case of brain sections. Molecular imaging of major classes of glycerophospholipids, sphingolipids and glycerolipids has been performed with a spatial resolution down to 6 μm per pixel and with high mass accuracy. The characteristic distributions of lipids and pheromones have been compared and imaged from different sex-specific biological replicates. Lipids, neuropeptides and small metabolites from the very small coronal head sections of *D. melanogaster* were identified from different biological replicates, which can explain their molecular and morphological identity in a reproducible manner. Our method will be applied in the future to study the mechanism of action and effects of e.g. orally administered drugs, metabolites and pesticides.

Using AP-SMALDI for small-sample analysis has a great potential where measurement can be carried out without the overlapping of laser spots and without much damage to the tissue sample down to a spatial resolution of 5 μm per pixel.

Our results suggest that AP-SMALDI conditions are suitable for obtaining quantifiable and distinguishable images of lipids, small metabolites, peptides, and pheromones from *D. melanogaster* by high-resolution MS imaging in order to obtain a better understanding of the biology of this important model organism.

Table 4
Metabolites detected in AP-SMALDI MSI analyses of the head of *Drosophila melanogaster* in positive-ion mode using DHB as a matrix. Structures were assigned based on accurate mass and literature data.

Formula	[M]	$[M+Na]^{+}_{calc}$	$[M+K]^{+}_{calc}$	$[M+H]^{+}_{calc}$	$[M+H]^{+}$,Observed M/Z	RMSE of $[M+H]^{+}_{obs.}$/ppm	Identity
Uric acid related							
$C_5H_4N_4O_3$	168.0277924	191.0175617	206.99150	169.03562	169.03581	1.14	Uric acid
$C_5H_4N_4O_2$	152.0328774	175.0226467	190.99658	153.04070	153.04060	−0.67	Xanthine
$C_5H_5N_5O$	151.0488614	174.0386307	190.01257	152.05669	152.05660	−0.57	Guanine
$C_{10}H_{13}N_5O_5$	283.0911214	306.0808907	322.05483	284.09895	284.09865	−1.05	Guanosine
$C_9H_{11}N_5O_3$	237.0856414	260.0754107	276.04935	238.09347	238.09370	0.99	Biopterin
$C_{10}H_{12}N_4O_5$	268.0802224	291.0699917	307.04393	269.08805	269.08852	1.76	Inosine
$C_{10}H_{14}N_5O_7P$	347.0625394	370.0523087	386.02625	348.07036	348.06985	−1.48	AMP
Tryptophan pathway metabolites							
$C_{11}H_{12}N_2O_2$	204.0893294	227.0790987	243.05304	205.09715	205.09690	−1.25	Tryptophan
$C_{11}H_{12}N_2O_3$	220.0842444	243.0740137	259.04795	221.09207	221.09188	−0.86	Hydroxytryptophan
$C_{10}H_{12}N_2O_3$	208.0842444	231.0740137	247.04795	209.09207	209.09188	−0.91	Kynurenine
Osmolytes							
$C_8H_{20}NO_6P$	257.102827	280.09260	296.06653	258.11065	258.11075	0.38	Choline glycerophosphate
Pyrimidines							
$C_4H_5N_3O$	111.0427134	134.0324827	150.00642	112.05054	112.05075	1.89	Cytosine
Miscellaneous metabolites							
$C_5H_9NO_4$	147.0526104	170.0423797	186.01632	148.06044	148.06042	−0.11	Glutamate
$C_5H_{10}N_2O_3$	146.0685944	169.0583637	185.03230	147.07642	147.07634	−0.54	Glutamine
$C_5H_{11}NO_2$	117.0784304	140.0681997	156.04214	118.08626	118.08640	1.23	Valine
$C_{20}H_{33}N_3O_3$	363.2516434	386.2414127	402.21535	364.25947	364.25982	0.97	Tetradecadienyl histidine
$C_{10}H_{14}N_5O_8P$	363.0574544	386.0472237	402.02116	364.06528	364.06568	1.11	GMP
$C_{20}H_{35}NO$	305.2713154	328.2610847	344.23502	306.27914	306.27865	−1.61	Clavepictine B
$C_{10}H_{26}N_4$	202.2151974	225.2049667	241.17890	203.22302	203.22285	−0.85	Spermine

*Reference: Kamleh, M. A.; Hobani, Y.; Dow, J. A. T.; Zheng, L.; Watson, D. G. *FEBS Journal* **2009**, *276*, 6798–6809.

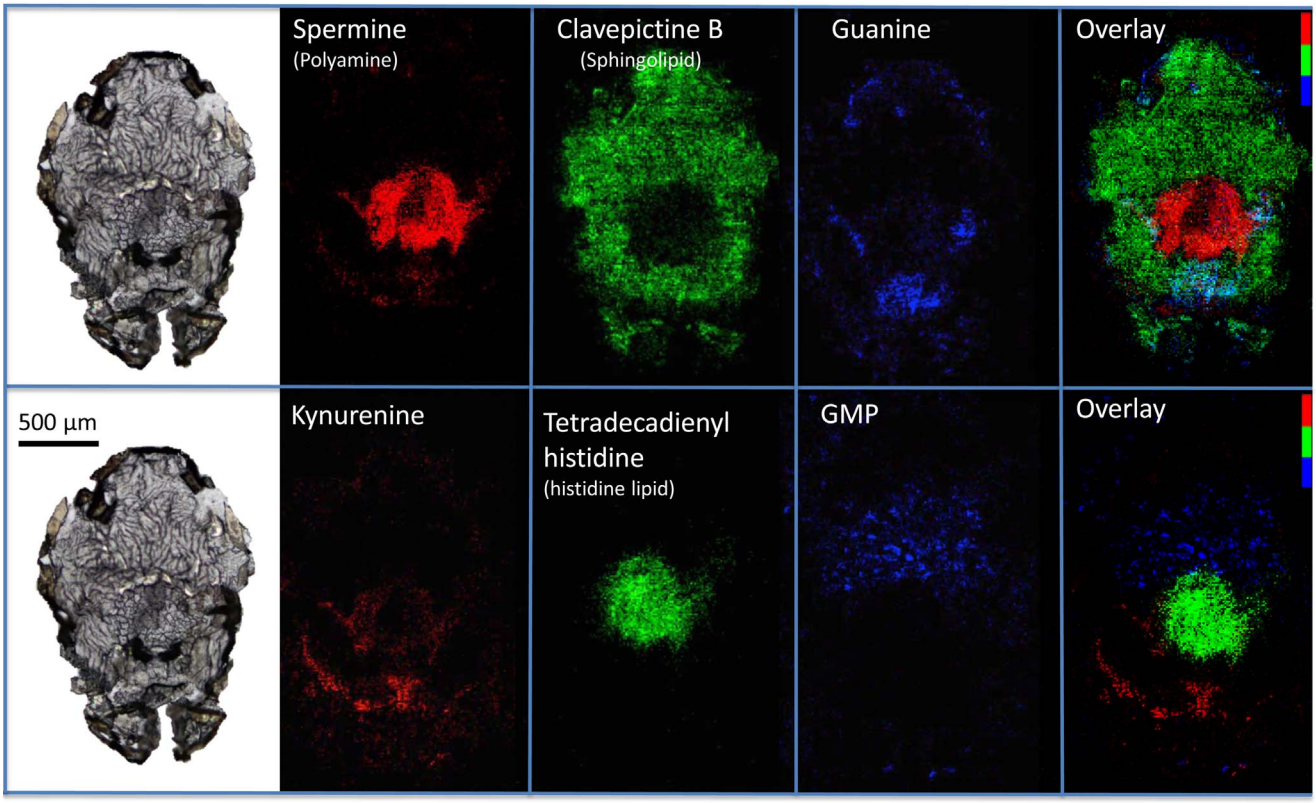

Fig. 12. Six different metabolites within the mass range of (m/z = 80-400), imaged with 204 × 240 pixels from the upper part of a female *D. melanogaster* axial brain section in positive-ion mode with a spatial resolution of 5 µm/pixel, using DHB as a matrix. The rightmost images show the RGB overlays of the three metabolites to their left.

Competing financal interest

S.M.K., J.P. and K.B. declare to have no competing financial interests. B.S. is a consultant of TransMIT GmbH, manufacturer of the AP-SMALDI10 ion source which was used for the reported studies.

Acknowledgements

We wish to thank Dr. Johannes Strauss and Prof. Reinhard Lakes-Harlan, Institute of Integrative Sensory Physiology, Justus Liebig University Giessen, for providing *Drosophila melanogaster* w118. The work was supported by the German Federal State of Hesse as part of the LOEWE research focus “Insect Biotechnology” and by the German Research Foundation (BE 1540/23-1 within SPP 1710 and Sp314/13-1).

Appendix A. Supplementary data

Supplementary data associated with this article can be found, in the online version, at http://dx.doi.org/10.1016/j.ijms.2017.04.001.

References

[1] M.D.W. Piper, D. Skorupa, L. Partridge, Diet, metabolism and lifespan in Drosophila, Exp. Gerontol. 40 (11) (2005) 857–862.
[2] S.L. Helfand, B. Rogina, Molecular genetics of aging in the fly: is this the end of the beginning? Bioessays 25 (2) (2003) 134–141.
[3] K.N. Bharucha, The epicurean fly: using drosophila melanogaster to study metabolism, Pediatr. Res. 65 (2) (2009) 132–137.
[4] K. Schwamborn, R.M. Caprioli, MALDI imaging mass spectrometry–painting molecular pictures, Mol. Oncol. 4 (6) (2010) 529–538.
[5] Y. Hsieh, J. Chen, W.A. Korfmacher, Mapping pharmaceuticals in tissues using MALDI imaging mass spectrometry, J. Pharmacol. Toxicol. Methods 55 (2) (2007) 193–200.
[6] U. Loizides-Mangold, On the future of mass-spectrometry-based lipidomics, FEBS J. 280 (12) (2013) 2817–2829.
[7] P. Chaurand, S. Schwartz, M. Reyzer, Caprioli R: imaging mass spectrometry: principles and potentials, Toxicol. Pathol. 33 (1) (2005) 92–101.
[8] D.R. Bhandari, M. Schott, A. Römpp, A. Vilcinskas, B. Spengler, Metabolite localization by atmospheric pressure high-resolution scanning microprobe matrix-assisted laser desorption/ionization mass spectrometry imaging in whole-body sections and individual organs of the rove beetle Paederus riparius, Anal. Bioanal. Chem. 407 (8) (2014) 2189–2201.
[9] A. Svatoš, Mass spectrometric imaging of small molecules, Trends Biotechnol. 28 (8) (2010) 425–434.
[10] A.-C. Niehoff, H. Kettling, A. Pirkl, Y.N. Chiang, K. Dreisewerd, J.Y. Yew, Analysis of drosophila lipids by matrix-assisted laser desorption/ionization mass spectrometric imaging, Anal. Chem. 86 (22) (2014) 11086–11092.
[11] T.-H. Wang, C.-H. Jian, Y.-K. Hsieh, F.-N. Wang, C.-F. Wang, Spatial distributions of inorganic elements in honeybees (Apis mellifera L.) and possible relationships to dietary habits and surrounding environmental pollutants, J. Agric. Food Chem. 61 (21) (2013) 5009–5015.
[12] S.M. Khalil, A. Römpp, J. Pretzel, K. Becker, B. Spengler, Phospholipid topography of whole-body sections of the anopheles stephensi mosquito, characterized by high-resolution atmospheric-pressure scanning microprobe matrix-assisted laser desorption/ionization mass spectrometry imaging, Anal. Chem. 87 (22) (2015) 11309–11316.
[13] D. Gode, D.A. Volmer, Lipid imaging by mass spectrometry–a review, The Analyst 138 (5) (2013) 1289.
[14] Y.P.M. van der Meer-Janssen, J. van Galen, J.J. Batenburg, J.B. Helms, Lipids in host-pathogen interactions: pathogens exploit the complexity of the host cell lipidome, Prog. Lipid Res. 49 (1) (2010) 1–26.
[15] J.-F. Ferveur, G. Sureau, Simultaneous influence on male courtship of stimulatory and inhibitory pheromones produced by live sex-mosaic drosophila melanogaster, Proc. R. Soc. Lond. B: Biol. Sci. 263 (1373) (1996) 967–973.
[16] J.Y. Yew, K. Dreisewerd, H. Luftmann, J. Müthing, G. Pohlentz, E.A. Kravitz, A new male sex pheromone and novel cuticular cues for chemical communication in drosophila, Curr. Biol. 19 (15) (2009) 1245–1254.
[17] L. Guan Xue, G. Cestra, G. Shui, A. Kuhrs, B. Schittenhelm Ralf, E. Hafen, F.G. van der Goot, C. Robinett Carmen, M. Gatti, M. Gonzalez-Gaitan, Biochemical membrane lipidomics during drosophila development, Dev. Cell 24 (1) (2013) 98–111.
[18] M. Carvalho, J.L. Sampaio, W. Palm, M. Brankatschk, S. Eaton, A. Shevchenko, Effects of diet and development on the Drosophila lipidome, Mol. Syst. Biol. 8 (2012) 600.
[19] L.A. Hammad, B.S. Cooper, N.P. Fisher, K.L. Montooth, J.A. Karty, Profiling and quantification of Drosophila melanogaster lipids using liquid chromatography/mass spectrometry, Rapid Commun. Mass Spectrom. 25 (19) (2011) 2959–2968.
[20] V.R. Chintapalli, M. Al Bratty, D. Korzekwa, D.G. Watson, J.A.T. Dow, Mapping an atlas of tissue-specific drosophila melanogaster metabolomes by high resolution mass spectrometry, PLoS One 8 (10) (2013) e78066.
[21] F. Kaftan, V. Vrkoslav, P. Kynast, P. Kulkarni, S. Böcker, J. Cvačka, M. Knaden, A. Svatoš, Mass spectrometry imaging of surface lipids on intactDrosophila melanogasterflies, J. Mass Spectrom. 49 (3) (2014) 223–232.
[22] V. Vrkoslav, A. Muck, J. Cvačka, A. Svatoš, MALDI imaging of neutral cuticular lipids in insects and plants, J. Am. Soc. Mass Spectrom. 21 (2) (2010) 220–231.
[23] U.B. Pandey, C.D. Nichols, Human disease models in drosophila melanogaster and the role of the fly in therapeutic drug discovery, Pharmacol. Rev. 63 (2) (2011) 411–436.
[24] Z. Xun, R.A. Sowell, T.C. Kaufman, D.E. Clemmer, Protein expression in a drosophila model of Parkinson’s disease, J. Proteome Res. 6 (1) (2007) 348–357.
[25] J. Hanrieder, N.T.N. Phan, M.E. Kurczy, A.G. Ewing, Imaging mass spectrometry in neuroscience, ACS Chem. Neurosci. 4 (5) (2013) 666–679.
[26] M. Altstein, D. Nässel, Neuropeptide signaling in insects, in: T. Geary, A. Maule (Eds.), Neuropeptide Systems as Targets for Parasite and Pest Control, vol. 692, Springer US, 2010, pp. 155–165.
[27] S. Neupert, H.A.D. Johard, D.R. Nässel, R. Predel, Single-cell peptidomics of drosophila melanogaster neurons identified by Gal4-driven fluorescence, Anal. Chem. 79 (10) (2007) 3690–3694.
[28] S.C.P. Renn, J.H. Park, M. Rosbash, J.C. Hall, P.H. Taghert, A pdf neuropeptide gene mutation and ablation of PDF neurons each cause severe abnormalities of behavioral circadian rhythms in drosophila, Cell 99 (7) (1999) 791–802.
[29] M.A. Carlsson, M. Diesner, J. Schachtner, D.R. Nässel, Multiple neuropeptides in the Drosophila antennal lobe suggest complex modulatory circuits, J. Comp. Neurol. 518 (16) (2010) 3359–3380.
[30] J.Y. Yew, Y. Wang, N. Barteneva, S. Dikler, K.K. Kutz-Naber, L. Li, E.A. Kravitz, Analysis of neuropeptide expression and localization in adult drosophila melanogaster central nervous system by affinity cell-capture mass spectrometry, J. Proteome Res. 8 (3) (2009) 1271–1284.
[31] R. Predel, C. Wegener, W.K. Russell, S.E. Tichy, D.H. Russell, R.J. Nachman, Peptidomics of CNS-associated neurohemal systems of adult Drosophila melanogaster: a mass spectrometric survey of peptides from individual flies, J. Comp. Neurol. 474 (3) (2004) 379–392.
[32] G. Baggerman, A. Cerstiaens, A. De Loof, L. Schoofs, Peptidomics of the larval Drosophila melanogaster central nervous system, J. Biol. Chem. 277 (43) (2002) 40368–40374.
[33] J.P. Salisbury, K.J. Boggio, Y.-W.A. Hsu, J. Quijada, A. Sivachenko, G. Gloeckner, P.J. Kowalski, M.L. Easterling, M. Rosbash, J.N. Agar, A rapid MALDI-TOF mass spectrometry workflow for Drosophila melanogaster differential neuropeptidomics, Mol. Brain 6 (1) (2013) 1–15.
[34] N.T.N. Phan, J.S. Fletcher, P. Sjövall, A.G. Ewing, ToF-SIMS imaging of lipids and lipid related compounds in Drosophila brain, Surf. Interface Anal.: SIA 46 (Suppl. 1) (2014) 123–126.
[35] M. Strohalm, Ji Strohalm, F. Kaftan, Ls Krásný, M. Volný, P. Novák, K. Ulbrich, Vr Havlíček, Poly[N-(2-hydroxypropyl)methacrylamide]-based tissue-embedding medium compatible with MALDI mass spectrometry imaging experiments, Anal. Chem. 83 (13) (2011) 5458–5462.
[36] R. Chen, L. Hui, R.M. Sturm, L. Li, Three dimensional mapping of neuropeptides and lipids in crustacean brain by mass spectral imaging, J. Am. Soc. Mass Spectrom. 20 (6) (2009) 1068–1077.
[37] N. Zaima, N. Goto-Inoue, T. Hayasaka, M. Setou, Application of imaging mass spectrometry for the analysis of Oryza sativa rice, Rapid Commun. Mass Spectrom. 24 (18) (2010) 2723–2729.
[38] M. Stoeckli, D. Staab, A. Schweitzer, Compound and metabolite distribution measured by MALDI mass spectrometric imaging in whole-body tissue sections, Int. J. Mass spectrom. 260 (2–3) (2007) 195–202.
[39] R.J. Goodwin, S.R. Pennington, A.R. Pitt, Protein and peptides in pictures: imaging with MALDI mass spectrometry, Proteomics 8 (18) (2008) 3785–3800.
[40] M. Karas, F. Hillenkamp, Laser desorption ionization of proteins with molecular masses exceeding 10,000 daltons, Anal. Chem. 60 (20) (1988) 2299–2301.
[41] K. Tanaka, H. Waki, Y. Ido, S. Akita, Y. Yoshida, T. Yoshida, T. Matsuo, Protein and polymer analyses up to m/z 100 000 by laser ionization time-of-flight mass spectrometry, Rapid Commun. Mass Spectrom. 2 (8) (1988) 151–153.
[42] K. Chughtai, R.M.A. Heeren, Mass spectrometric imaging for biomedical tissue analysis, Chem. Rev. 110 (5) (2010) 3237–3277.
[43] B.K. Kaletaş, I.M. van der Wiel, J. Stauber, J.D. Lennard, C. Güzel, J.M. Kros, T.M. Luider, R.M.A. Heeren, Sample preparation issues for tissue imaging by imaging MS, Proteomics 9 (10) (2009) 2622–2633.
[44] R.T. Steven, A.M. Race, J. Bunch, Para-nitroaniline is a promising matrix for MALDI-MS imaging on intermediate pressure MS systems, J. Am. Soc. Mass Spectrom. 24 (5) (2013) 801–804.
[45] R. Steven, A. Race, J. Bunch, Para-nitroaniline is a promising matrix for MALDI-MS imaging on intermediate pressure MS systems, J. Am. Soc. Mass Spectrom. 24 (5) (2013) 801–804.
[46] A. Römpp, B. Spengler, Mass spectrometry imaging with high resolution in mass and space, Histochem. Cell Biol. 139 (6) (2013) 759–783.
[47] S. Guenther, M. Koestler, O. Schulz, B. Spengler, Laser spot size and laser power dependence of ion formation in high resolution MALDI imaging, Int. J. Mass spectrom. 294 (1) (2010) 7–15.
[48] C. Paschke, A. Leisner, A. Hester, K. Maass, S. Guenther, W. Bouschen, B. Spengler, Mirion—a software package for automatic processing of mass spectrometric images, J. Am. Soc. Mass Spectrom. 24 (8) (2013) 1296–1306.
[49] A. Römpp, S. Guenther, Y. Schober, O. Schulz, Z. Takats, W. Kummer, B. Spengler, Histology by mass spectrometry: label-free tissue characterization obtained from high-accuracy bioanalytical imaging, Angew. Chem. Int. Ed. 49 (22) (2010) 3834–3838.

[50] V.P. Skipski, R.F. Peterson, M. Barclay, Quantitative analysis of phospholipids by thin-layer chromatography, Biochem. J. 90 (2) (1964) 374–378.
[51] S. Gamo, A. Kawabe, H. Kohara, H. Yamaguchi, Y. Tanaka, S. Yagi, Fast atom bombardment tandem mass spectrometric analysis of phospholipids in Drosophila melanogaster, J. Mass Spectrom. 34 (6) (1999) 590–600.
[52] A. Römpp, S. Guenther, Z. Takats, B. Spengler, Mass spectrometry imaging with high resolution in mass and space (HR2 MSI) for reliable investigation of drug compound distributions on the cellular level, Anal. Bioanal. Chem. 401 (1) (2011) 65–73.
[53] E.L. Arrese, J.L. Soulages, Insect fat body: energy, metabolism, and regulation, Annu. Rev. Entomol. 55 (2010) 207–225.
[54] J.S.R. Chin, S.R. Ellis, H.T. Pham, S.J. Blanksby, K. Mori, Q.L. Koh, W.J. Etges, J.Y. Yew, Sex-specific triacylglycerides are widely conserved in Drosophila and mediate mating behavior, eLife 3 (2014) e01751.
[55] J. Stiban, R. Tidhar, A. Futerman, Ceramide synthases: roles in cell physiology and signaling, in: C. Chalfant, M. Poeta (Eds.), Sphingolipids as Signaling and Regulatory Molecules, vol. 688, Springer, New York, 2010, pp. 60–71.
[56] M.A. Masood, C. Yuan, J.K. Acharya, T.D. Veenstra, J. Blonder, Quantitation of ceramide phosphorylethanolamines containing saturated and unsaturated sphingoid base cores, Anal. Biochem. 400 (2) (2010) 259–269.
[57] C. Yuan, R.P. Rao, N. Jesmin, T. Bamba, K. Nagashima, A. Pascual, T. Preat, E. Fukusaki, U. Acharya, J.K. Acharya, CDase is a pan-ceramidase in Drosophila, Mol. Biol. Cell 22 (1) (2010) 33–43.
[58] S. Hebbar, W.D. Schulz, U. Sauer, D. Schwudke, Laser capture microdissection coupled with on-column extraction LC-MSn enables lipidomics of fluorescently labeled drosophila neurons, Anal. Chem. 86 (11) (2014) 5345–5352.
[59] K. Meylaers, E. Clynen, D. Daloze, A. DeLoof, L. Schoofs, Identification of 1-lysophosphatidylethanolamine (C16:1) as an antimicrobial compound in the housefly, Musca domestica, Insect Biochem. Mol. Biol. 34 (1) (2004) 43–49.
[60] V.R. Chintapalli, M. Al Bratty, D. Korzekwa, D.G. Watson, J.A.T. Dow, Mapping an atlas of tissue-specific *Drosophila melanogaster* metabolomes by high resolution mass spectrometry, PLoS One 8 (10) (2013) e78066.
[61] V.R. Chintapalli, J. Wang, J.A.T. Dow, Using FlyAtlas to identify better Drosophila melanogaster models of human disease, Nat. Genet. 39 (6) (2007) 715–720.
[62] P.S. Shekhawat, S. Sonne, A.L. Carter, D. Matern, V. Ganapathy, Enzymes involved in L-carnitine biosynthesis are expressed by small intestinal enterocytes in mice: implications for gut health, J. Crohn Colitis 7 (6) (2013) e197–e205.
[63] H. Guillou, D. Zadravec, P.G.P. Martin, A. Jacobsson, The key roles of elongases and desaturases in mammalian fatty acid metabolism: insights from transgenic mice, Prog. Lipid Res. 49 (2) (2010) 186–199.
[64] J. Overgaard, A. Tomčala, J.G. Sørensen, M. Holmstrup, P.H. Krogh, P. Šimek, V. Koštál, Effects of acclimation temperature on thermal tolerance and membrane phospholipid composition in the fruit fly Drosophila melanogaster, J. Insect Physiol. 54 (3) (2008) 619–629.
[65] R.C. Hardie, P. Raghu, Visual transduction in drosophila, Nature 413 (6852) (2001) 186–193.
[66] B. Baer, E.D. Morgan, P. Schmid-Hempel, A nonspecific fatty acid within the bumblebee mating plug prevents females from remating, Proc. Natl. Acad. Sci. 98 (7) (2001) 3926–3928.
[67] M. Ueyama, T. Chertemps, C. Labeur, C. Wicker-Thomas, Mutations in the desat1 gene reduces the production of courtship stimulatory pheromones through a marked effect on fatty acids in Drosophila melanogaster, Insect Biochem. Mol. Biol. 35 (8) (2005) 911–920.
[68] C. Everaerts, J.-P. Farine, M. Cobb, J.-F. Ferveur, Drosophila cuticular hydrocarbons revisited: mating status alters cuticular profiles, PLoS One 5 (3) (2010) e9607.
[69] R.W. Howard, G.J. Blomquist, Ecological, behavioral, and biochemical aspects of insect hydrocarbons, Annu. Rev. Entomol. 50 (1) (2005) 371–393.
[70] Y. Shikichi, S. Shankar, J.Y. Yew, K. Mori, Synthesis and bioassay of the eight analogues of the CH503 male pheromone (3-Acetoxy-11, 19-octacosadien-1-ol) of the drosophila melanogaster fruit fly, Biosci. Biotechnol. Biochem. 77 (9) (2013) 1931–1938.
[71] B.E. Noyes, F.N. Katz, M.H. Schaffer, Identification and expression of the Drosophila adipokinetic hormone gene, Mol. Cell. Endocrinol. 109 (2) (1995) 133–141.
[72] R.J. Siviter, G.M. Coast, Å.M.E. Winther, R.J. Nachman, C.A.M. Taylor, A.D. Shirras, D. Coates, R.E. Isaac, D.R. Nässel, Expression and functional characterization of a Drosophila neuropeptide precursor with homology to mammalian preprotachykinin a, J. Biol. Chem. 275 (30) (2000) 23273–23280.
[73] R.S. Hewes, E.C. Snowdeal, M. Saitoe, P.H. Taghert, Functional redundancy of FMRFamide-Related peptides at the Drosophila larval neuromuscular junction, J. Neurosci. 18 (18) (1998) 7138–7151.
[74] M. Heisenberg, What do the mushroom bodies do for the insect brain? An introduction, Learn. Mem. 5 (1) (1998) 1–10.
[75] M.A. Kamleh, Y. Hobani, J.A.T. Dow, L. Zheng, D.G. Watson, Towards a platform for the metabonomic profiling of different strains of Drosophila melanogaster using liquid chromatography-Fourier transform mass spectrometry, FEBS J. 276 (22) (2009) 6798–6809.
[76] L.J. Marton, Polyamines and brain tumors, Natl. Cancer Inst. Monogr. 46 (1977) 127–131.
[77] A. Kumar, M. Taylor, T. Altabella, A.F. Tiburcio, Recent advances in polyamine research, Trends Plant Sci. 2 (4) (1997) 124–130.
[78] M. Kliman, N. Vijayakrishnan, L. Wang, J.T. Tapp, K. Broadie, J.A. McLean, Structural mass spectrometry analysis of lipid changes in a Drosophila epilepsy model brain, Mol. Biosyst. 6 (6) (2010) 958–966.
[79] E.C. Berglund, M.A. Makos, J.D. Keighron, N. Phan, M.L. Heien, A.G. Ewing, Oral administration of methylphenidate blocks the effect of cocaine on uptake at the drosophila dopamine transporter, ACS Chem. Neurosci. 4 (4) (2013) 566–574.